SUPPLEMENTAL MATERIAL

Extended Methods

Mice

All animal experiments were carried out following the Guide for the Care and Use of Laboratory Animals (National Institutes of Health publication 85–23, revised 1996) and were approved by the Institutional Animal Care and Use Committee at Shanghai Jiao Tong University School of Medicine and Fujian Medical University. Male wild-type C57BL/6 mice aged 8–10 weeks were obtained from Beijing Vital River Laboratory Animal Technology Co., Ltd. Rnf149 conventional knockout (KO) mice were generated by disrupting the *Rnf149* gene using CRISPR–Cas9 gene editing at Cyagen Biosciences Inc (Suzhou, Jiangsu, China). Cas9 protein and two gRNAs (gRNA1: GATAGACATCTTTATAGTTCTGG, gRNA2: GGAAGTTTAGGAGTTCTATAAGG) were injected into fertilized eggs. The resulting embryos were transferred to recipient female mice to obtain F0 founder mice. The genotype of conventional knockout mice was confirmed by PCR using two pairs of primers (Common forward primer: 5'-TAGTGATCACAGAAGAGCTCTCACA-3'; reverse primer for mutant allele: 5'-AGTGGAAAAGCTGGTTTAGAATCAC-3'; reverse primer for wild-type allele: 5'-AGTGAGAAAATCACCAGGAACTGT-3') and sequencing. *Rnf149* heterozygous (+/-) mice were then crossed with *Rnf149* (+/-) mice to produce *Rnf149* null (-/-) (RNF149 knockout, termed RNF149KO) mice, with *Rnf149* (+/+) littermates serving as wild-type (WT) controls. All mice were maintained on C57BL/6 background, and male mice aged 8 to 10 weeks were used in this study. Given the well-established association of male gender with a heightened risk for cardiovascular diseases and the recognized protective effects of estrogen against inflammation and pathological remodeling following MI, we exclusively conducted all animal experiments using male mice to avoid potential impacts of sex-based differences in response to myocardial ischemia and to ensure the induction of robust myeloid immune responses and cardiac remodeling following ischemic challenge. Male mice were also utilized in our prior studies focusing on myeloid immune responses in the context of myocardial ischemia[5-8]. The ARRIVE 2.0 guidelines were followed for animal experiments. Mice were housed in a specific pathogen-free facility with a 12-h light/dark cycle and free access to food and water.

In vivo randomization and blinding procedures

The sample size of mice was calculated based on a priori analysis by G-Power 3.1.9.2 software (two-tailed, statistical power=80%, and α=0.05; the effect size was determined based on preliminary experimental results and literature review). A priori power analysis indicated that a minimum of 5 mice per group is required for a comparative study. Randomization and allocation concealment were executed. Using a random number generator, the mice were randomly divided into groups. All animal experiments were performed and analyzed in a blinded fashion. Data collection and analysis were carried out by researchers who were unaware of the group assignment or treatment administered to the animals.

Animal models and *in vivo* interventions

Male mice, aged 8 to 10 weeks, were subjected to either permanent (MI) or transient (IR) ligation of the left anterior descending artery (LAD), while control group underwent a sham operation without ligation. In brief, mice were initially lightly anesthetized with diethyl ether, intubated using a 22-gauge tube, and then placed under full anesthesia with 1.5–2% isoflurane, while being mechanically ventilated with a specialized small rodent respirator. A left thoracotomy was performed between the third and fourth intercostal space to gain access to the left ventricle. The LAD segment, approximately 1.5 mm to 2 mm lower than the tip of the left auricle, was permanently ligated using an 8-0 monofilament nylon suture. Complete occlusion of the LAD was confirmed by the blanching of myocardial tissue distal to the ligature. Subsequently, the chest wall was closed, and air from the thorax was evacuated through a pleural catheter. For the induction of IR, a slipknot was fashioned around the LAD using a 7-

0 silk suture against a PE10 tubing. After 45 minutes of ligation, the slipknot was released to allow reperfusion. The Sham-operated mice underwent the same surgical procedure, excluding the LAD ligation. Mice that died within 6 hours after surgery due to acute heart failure were excluded from the study; mice with echocardiographic ejection fraction (EF) greater than 50% on day 1 after surgery were considered surgical failure and excluded from the present study. Daily monitoring of all mice was carried out after MI. Following the sham or LAD ligation surgery, cardiac function was evaluated using echocardiography, and heart samples were collected at various time points for subsequent experiments.

Recombinant adeno-associated virus (AAV) and intra-bone marrow (BM) targeting interference: A recombinant AAV vector carrying a macrophage-specific RNF149 deletion plasmid or a negative control (NC) plasmid containing scramble shRNA was generated by Hanbio Biotechnology (Shanghai, China). The AAV2 viral vector harbors a macrophage-specific F4/80 promoter, a miR30-based shRNA targeting RNF149[14], a cytomegalovirus promoter, and an enhanced GFP reporter. The nucleotide shRNA of mouse RNF149 was cloned using the following sequence: 5'-GAACAGGAAACATAGTCGTCATTAT-3'. AAV-F4/80-shRNF149 viral titer of 1.2×10^{13} vector genomes (vg)/mL and AAV-F4/80-NC viral titer of 1.2×10^{13} vg/mL were used in the study. For local delivery, 60 μL of AAV2-F4/80-shRNF149 or AAV2-F4/80-NC were intraosseously injected into BM of 8-week-old male C57BL/6 wild-type mice, as previously described[15-16]. RNF149 knockdown in macrophages was confirmed by real-time PCR (Figure S8). For the IFNGR1 knockdown study, a recombinant AAV vector carrying a macrophage-specific IFNGR1 deletion plasmid or a negative control (NC) plasmid containing scramble shRNA was generated by Hanbio Biotechnology (Shanghai, China). The AAV2 viral vector harbors a macrophage-specific F4/80 promoter, a miR30-based shRNA targeting IFNGR1[14], a cytomegalovirus promoter, and an enhanced GFP reporter. The nucleotide shRNA of mouse IFNGR1 was cloned using the following sequence: 5'-AAGAACAGCTCTCCGTCCTCGTATT-3'. AAV-F4/80-shIFNGR1 viral titer of 1.2×10^{13} vector genomes (vg)/mL and AAV-F4/80-NC viral titer of 1.2×10^{13} vg/mL were used in the study. For local delivery, 60 μL of AAV2-F4/80-shIFNGR1 or AAV2-F4/80-NC were intraosseously injected into BM of 8-week-old male WT and RNF149KO mice, as previously described[15-16]. IFNGR1 knockdown in BM-derived macrophages was confirmed by real-time PCR on day 28 after AAV injection (Figure S15).

Adenovirus production and RNF149 gene delivery *in vivo*: adenovirus (Ad) plasmids carrying the full-length RNF149 coding sequence and adenovirus null control plasmids were constructed by Hanbio Biotechnology (Shanghai, China). Intramyocardial injections of AdRNF149 or Adnull were administered after LAD ligation at a dose of 1×10^9 pfu per mouse, as previously described[17,18]. Adnull is the adenovirus containing an empty macrophage CD68 promoter and functions as the control. RNF149 overexpression in macrophages was confirmed by real-time PCR (Figure S10).

Bone marrow transplantation (BMT)

CD45.1 strain mice were obtained from Cyagen Biosciences Inc (Suzhou, Jiangsu, China). BMT experiments were performed between WT (CD45.1) and RNF149KO (CD45.2) mice. Bone marrow (BM) cells were harvested from the femurs and tibias of 8-week-old male donor mice after euthanasia. Recipient male mice, also aged eight weeks, underwent lethal irradiation and were subsequently transplanted with BM cell suspensions comprising 100% $CD45.1^+$ or $CD45.2^+$ cells from the respective donors. To ensure uniform irradiation doses and minimize mobility, recipient mice were placed in a pie cage and exposed to two radiation doses, each amounting to 450 rad, administered four hours apart. Following the second irradiation, each recipient mouse received an injection of $5x10^6$ BM cells via the retro-orbital vein plexus. During the initial 14 days post-transplantation, these mice were housed in sterile cages and provided with food and water supplemented with antibiotics (Sulfatrim). Reconstitutions were assessed through flow cytometry analysis of peripheral blood. Eight weeks after the BMT, these mice were subjected to cardiac MI surgery.

Echocardiography

Transthoracic echocardiography was conducted using a Vevo 2100 instrument equipped with an MS-400 imaging transducer (VisualSonics, Toronto, ON, Canada), as previously described[5, 6, 8]. In detail, the mice were initially anesthetized with isoflurane in an enclosed chamber and then gently and securely immobilized on an echo pad in a supine position. The mice remained conscious, without anesthesia, during the echocardiographic imaging procedure to minimize potential data deviations. The heart rate was carefully maintained within the range of 500 to 600 bpm for all mice. Two-dimensional (2D) images were obtained in both the left ventricular short- and long-axis planes. Left ventricular end-diastolic volume (LVEDV) and end-systolic volume (LVESV) were calculated utilizing the biplane area-length method. Left ventricular ejection fraction (LVEF) was determined by applying the formula: LVEF = [(LVEDV-LVESV)/LVEDV] × 100%. The 2D-guided left ventricular M-mode tracings were recorded at the level of the papillary muscle, either from the short-axis or long-axis view, to measure left ventricular internal diameter at end-systole (LVID;s) and left ventricular internal diameter at end-diastole (LVID;d). Left ventricular fractional shortening (LVFS) was computed using the following formula: LVFS = [(LVID;d-LVID;s)/LVID;d] × 100%. The representative image for each group was chosen based on the mean value.

^{18}F-labeled fluorodeoxyglucose (^{18}F-FDG) positron emission tomography/computed tomography (PET/CT) scanning

The ^{18}F-FDG PET/CT was conducted to assess myocardial viability on day 28 after MI. PET/CT scanning and the analysis of images were performed using Mediso Medical Imaging Systems. Each mouse received a tail vein injection of 200μCi ^{18}F-FDG under 2% isoflurane inhalation anesthesia. A 10-minute static scanning was conducted 1 h after ^{18}F-FDG injection (for ^{18}F-FDG uptake), with mice in a prone position on the PET/CT scanner bed and maintained under 2% isoflurane inhalation anesthesia. Mice underwent overnight fasting before ^{18}F-FDG injection and remained static under isoflurane inhalation during the 1-hour waiting phase. The images were processed using the InterView™ FUSION software. Regions of interest (ROIs) were delineated over the heart guided by CT images. Tracer uptake was quantified using InterView™ FUSION software, and individual ^{18}F-FDG uptake in each mouse was calculated. The mean standardized uptake value (SUV) of ^{18}F-FDG was calculated by dividing the relevant ROI activity by the ratio of the injected dose to the body weight. The representative image for each group was chosen based on the mean value.

Human samples

Heart tissue samples from patients with acute MI and healthy controls were provided by Dr. Liliang Li from the Department of Forensic Medicine, School of Basic Medical Sciences, Fudan University. All procedures involving patient samples and tissue handling were approved by the Human Subjects Institutional Review Board at Ruijin Hospital. Myocardial tissue samples from the left ventricle were obtained at autopsy from five patients who died of cardiogenic shock or sudden death within three days after acute MI, and from five control subjects who had not displayed clinical or pathological indications of cardiac disease and died from non-cardiac causes such as trauma and car accident. Detailed clinical profiles of the MI patients and control subjects can be found in Table S10. The collected heart samples were fixed in 10% formalin, followed by paraffin embedding and sectioning at a thickness of 4 μm. These sections were then used for immunohistochemistry and immunofluorescence assays.

Histology

Mouse MI heart samples were fixed with 4% PFA, followed by embedding in paraffin and subsequent division into 4 μm transverse sections at distinct levels. Masson's trichrome and picrosirius red staining procedures were employed on the paraffin-embedded sections to evaluate the extent of cardiac fibrosis. Ten to fifteen images were systematically captured from randomly chosen fields in both infarct and non-infarct regions for each section. Image analysis was executed through the utilization of Image J software (National Institutes of Health).

Collagen density was calculated by determining the ratio of the positively stained area to the total scar area. To assess infarct size, Masson's trichrome staining was applied to serial heart cross sections acquired above the level of ligation site as well as at 0.5 mm intervals distal to the suture. The infarct size was quantified as a percentage of the necrotic area relative to the total left ventricular area. The representative image for each group was chosen based on the mean value.

Infarct size following IR injury was determined using Evans blue/TTC staining. Briefly, two days post-IR, mice were anesthetized, and the LAD was re-occluded at the previous ligation site. Subsequently, 2% Evans blue was injected into the LV cavity. The heart was promptly excised, washed, immediately frozen, and sliced into 1.2-mm sections. These sections were then incubated in a 1% 2,3,5-triphenyltetrazolium chloride (TTC) solution and digitally imaged. The areas stained with Evans blue, TTC (representing the area at risk, AAR), and the regions lacking TTC staining (indicating infarcted myocardium) were quantified using computerized planimetry via Image J software. Myocardial infarct size was expressed as a percentage of the infarct area relative to AAR, and the size of AAR was expressed as a percentage of the AAR relative to the total LV area. The representative image for each group was selected based on the mean value.

For infarct measurement, hearts were harvested and promptly frozen at -80°C. The frozen specimens were subsequently sectioned transversely into 1.2-mm-thick slices and stained with 1% TTC in PBS (pH 7.4) for 20 minutes in a 37°C water bath. Following fixation in 10% neutral buffered formaldehyde for 4 to 6 hours, both sides of each slice were photographed. Viable myocardial tissue exhibited a distinct brick-red hue, while infarcted regions displayed a characteristic pale white appearance. Quantitative analysis of infarct size and LV area was performed using automated planimetry facilitated by Image J software, with the extent of infarction expressed as a percentage relative to the total LV area. The representative image for each group was selected based on the mean value.

Immunohistochemistry

Immunohistochemistry assays were conducted on 4 μm paraffin-embedded mouse and human heart sections. To enhance the specificity of immunostaining, heat-induced antigen retrieval was performed on the deparaffinized heart sections. To prevent non-specific binding of the antibody to the tissues, the sections were blocked with 5% goat serum for 1 hour at room temperature. Primary antibody against RNF149 (Catalog #: PA5-110306, Invitrogen) was applied to the sections in a humidified chamber at 4 °C overnight. Subsequently, biotinylated secondary antibodies were applied, followed by the utilization of the VECTASTAIN ABC reagent (Catalog #: PK-4001, Vector Laboratories). Color development was achieved through the use of the DAB substrate (Catalog #: SK-4105, Vector Laboratories). Isotype-matched controls were employed to validate the specificity of staining generated by the primary antibody. In addition, negative controls involving the use of incubation buffer without the primary antibody were employed to identify any non-specific staining caused by the secondary reagents.

Immunofluorescence staining

Immunofluorescence experiments were conducted on 4 μm sections of paraffin-embedded human heart tissues and 8 μm sections from mouse cardiac cryostat samples. Briefly, these sections were initially blocked in 1x PBS solution containing 1% bovine serum albumin (BSA) for one hour at room temperature and then incubated with primary antibodies at 4°C overnight. To validate the specificity of the primary antibodies, IgG isotype control antibodies were employed as negative controls. Additionally, fluorescent-labeled secondary antibody-only controls were utilized to distinguish genuine target staining from the background. Afterward, the sections underwent a thorough washing with 1x PBS three times, followed by a two-hour incubation with appropriate fluorescent-labeled secondary antibodies at room temperature. Subsequently, the sections were counterstained with DAPI (4'6-diamidino-2-phenylindole) (Catalog #: D1306, Invitrogen), and then mounted with VECTASHIELD Anti-fade Mounting

Medium (Catalog #: H-1000-10, Vector Laboratories). The stained sections were visualized using a Zeiss 710 confocal microscope (Carl Zeiss), and image analysis was carried out using Image J software (National Institutes of Health). The representative image for each group was selected based on the mean value. The primary antibodies used for immunofluorescence included: Anti-F4/80 antibody (Catalog #: MCA497, AbDSerotec**),** Anti-Ly6G antibody (Catalog #: ab210204, Abcam), Anti-α-actinin antibody (Catalog #: A7811, Sigma-Aldrich), Anti-CD68 antibody (Catalog #: ab955, Abcam), Anti-RNF149 antibody (Catalog #: PA5-110306, Invitrogen), Anti-CD11b antibody (Catalog #: ab128797, Abcam), Anti-Collagen I antibody (Catalog #: ab34710, Abcam), Anti-CD31 antibody (Catalog #: 557355, BD Biosciences), Anti-α-SMA antibody (Catalog #: ab5694, Abcam), Anti-HMGB1 antibody (Catalog #: ab18256, Abcam). The secondary antibodies used were: Donkey anti-Rabbit Secondary Antibody, Alexa Fluor 488 (Catalog #: A-21206, Invitrogen), Goat anti-Rat Secondary Antibody, Alexa Fluor 594 (Catalog #: A-11007, Invitrogen), Goat anti-Mouse Secondary Antibody, Alexa Fluor Plus 647 (Catalog #: A32728TR, Invitrogen), Goat anti-Mouse Secondary Antibody, Alexa Fluor 594 (Catalog #: A-11005, Invitrogen), Donkey anti-Rat Secondary Antibody, Alexa Fluor 488 (Catalog #: A-21208, Invitrogen), Goat anti-Rabbit Secondary Antibody, Alexa Fluor 594 (Catalog #: A-11037, Invitrogen).

In situ detection of apoptosis

For the analysis of cardiomyocyte apoptosis, 8 μm thick frozen heart sections were fixed by 4% paraformaldehyde (PFA) and subsequently subjected to TUNEL staining employing the *In Situ* Cell Death Detection Kit-Fluorescein (Catalog #: 11684795910, Roche). Following this, the sections were co-stained with Anti-α-actinin antibody (Catalog #: A7811, Sigma-Aldrich) to specifically label cardiomyocytes. Subsequently, a Goat anti-Mouse Secondary Antibody, Alexa Fluor 594 (Catalog #: A-11005, Invitrogen) was applied as a secondary antibody. Cell nuclei were stained with DAPI (4'6-diamidino-2-phenylindole) (Catalog #: D1306, Invitrogen). A total of six to eight fields, randomly selected from the infarct, border, and remote areas of MI hearts, were observed for each cross section, under a Zeiss 710 confocal microscope (Carl Zeiss). Different regions of MI hearts were distinguished based on α-actinin staining patterns. The infarct area was characterized by a notable reduction of α-actinin staining. The border zone was defined as the immediate neighboring regions around the infarct area, representing the transition zones between infarcted and healthy myocardium. In the border zone, α-actinin staining appeared irregular or fragmented. The remote area was defined as the unaffected myocardium distant from the infarct area. In the remote region, α-actinin staining appeared normal, demonstrating intact cardiomyocyte structure and organization. The apoptotic index was calculated as the percentage of apoptotic cardiomyocytes (TUNEL/α-actinin double positive) relative to the total number of cardiomyocytes. The representative image for each group was chosen based on the mean value.

Preparation of bone marrow-derived macrophages (BMDMs)

For the isolation of BMDMs, total BM cells were flushed out from femur and tibia bones of adult male mice and were subsequently cultured in BMDM growth medium (RPMI 1640 supplemented with 10 ng/mL M-CSF (Catalog #: SRP3221, Sigma-Aldrich), 100 Units /mL penicillin/streptomycin, and 10% FBS). The medium was changed on day 3 of the culture. After 7 days of differentiation, mature BMDMs underwent stimulation with murine IFN-γ (Catalog #: 315-05, PeproTech) for macrophage polarized activation. Then, the cells were collected for phenotypic characterization and functional assays at indicated time points.

Cell culture and transfection

Isolation and culture of mouse BMDMs were performed as described previously. HEK293T cells were kindly provided by the Stem Cell Bank, Chinese Academy of Sciences (CAS) and cultured in DMEM containing 10 % FBS following the instructions supplied by CAS. In our study, HEK293T cells were maintained for up to 5 passages. Lipofectamine 3000 (Catalog #: L3000150, Invitrogen) was used for transfection of plasmids into HEK293T cells.

A DNA sequence encoding IFNGR1 (NM_000416) was cloned into the GV657 vector (CMV enhancer-MCS-3flag-polyA-EF1A-zsGreen-sv40-puromycin) (GeneChem, Shanghai) to create the Flag-IFNGR1 plasmid. The IFNGR1 (K277R, 279R, and 285R) mutant, in which lysine-277, 279, and 285 were replaced with arginine, were generated from the Flag-IFNGR1 plasmid using the QuikChange site-directed mutagenesis kit (Agilent). A DNA sequence encoding RNF149 (NM_173647-myc) was cloned into the GV658 vector (CMV enhancer-MCS-polyA-EF1A-zsGreen-sv40-puromycin) (GeneChem, Shanghai) to create the Myc-RNF149 plasmid. The mutant construct $RNF149^{H289A}$, in which His-289 was replaced with alanine, was generated from the Myc-RNF149 plasmid using the site-directed mutagenesis kit (Agilent). Subsequently, the DNA sequences of NM_173647 (del67-175 aa)-Myc and NM_173647 (del269-310 aa)-Myc were cloned into the GV658 vector (CMV enhancer-MCS-polyA-EF1A-zsGreen-sv40-puromycin) (GeneChem, Shanghai) to generate the PA domain (67-175 aa)-deletion mutant and the RING domain (269-310 aa)-deletion mutant of Myc-RNF149, respectively. The HA-Ubiquitin-WT, HA-Ubiquitin-K48 (all lysines mutated to arginine except for K48), and HA-Ubiquitin-K48R (K48 mutated to arginine) were inserted into the GV658 vector (CMV enhancer-MCS-polyA-EF1A-zsGreen-sv40-puromycin) (GeneChem, Shanghai). cDNA of mouse STAT1 (NM_001205313) were cloned into the pcDNA3.1 expression vector. A 2.4-kb mouse *Rnf149* promoter, which contained putative STAT1 binding sites, was amplified and cloned into the pGL3-Basic vector (Promega) to produce the 2.4-kb Rnf149-firefly reporter plasmid. Different fragments of *Rnf149* promoter were inserted into pGL3-Basic vector to yield various truncated Rnf149-firefly reporter plasmids. pRL-TK vector (constitutively expressing Renilla luciferase) was purchased from Promega. All plasmids were verified by DNA sequencing.

The following chemicals reagents were used: cycloheximide (CHX, 50 μg/mL) (Catalog #: C4859, Sigma-Aldrich), Recombinant murine IFN-γ (Catalog #: 315-05, PeproTech), MG132 (20 μg/mL) (Catalog #: M8699, Sigma-Aldrich).

Cell preparation for flow cytometry

The mice were subjected to full anesthesia, following which their hearts were rapidly excised and perfused with ice-cold PBS to eliminate blood cells. Subsequently, the left ventricles from sham-operated mice and the infarct as well as border regions of MI hearts were excised, weighed, minced, and enzymatically digested in a 1x PBS buffer containing collagenase type II, DNase I, and elastase (all obtained from Worthington Biochemical Corporation). This digestion process occurred over the course of 1 hour at 37 °C with gentle agitation. Following digestion, the heart tissues were gently triturated and passed through a 70-μm cell strainer. Leukocytes were enriched utilizing 37-70% Percoll density gradient centrifugation. The collected cells were washed and subsequently suspended in a 1x PBS buffer supplemented with sterile 3% FBS and 1% BSA.

Flow cytometry and cell sorting

Cardiac immune cells: Initially, single-cell suspensions were incubated with anti-murine CD16/32 antibody (Catalog #: 14-0161-82, eBioscience) to prevent non-specific antibody binding to Fc gamma receptors. Subsequently, cells were labeled with a combination of fluorophore-conjugated antibodies targeting specific surface markers. In multicolor flow cytometry, a combination of isotype and FMO controls was employed to determine non-specific antibody binding and background fluorescence and to set gates for negative populations for each fluorochrome separately, as deemed necessary. For the analyses in Figure 4A, the antibody panel included CD45-Alexa Fluor 700 (clone 30-F11, Catalog #: 103128, Biolegend), CD11b-BV650 (clone M1/70, Catalog #: 101259, Biolegend), Ly6G-BV510 (clone 1A8, Catalog #: 127633, Biolegend), F4/80-PE (clone BM8, Catalog #: 123110, Biolegend), Ly6C-PE-CY7 (clone HK1.4, Catalog #: 25-5932-82, eBioscience), CD64-BV421 (clone X54-5/7.1, Catalog #: 139309, Biolegend), MHC-II-FITC (clone M5/114.15.2, Catalog #: 107605, Biolegend), CCR2-Alexa Fluor 647 (clone Y15-488.rMAb, Catalog #: 568347, BD). For the analyses in Figure 5K, Figure 7B, and Figure S14C, the antibody panel included CD45-

Alexa Fluor 700 (clone 30-F11, Catalog #: 103128, Biolegend), CD11b-BV650 (clone M1/70, Catalog #: 101259, Biolegend), Ly6G-BV510 (clone 1A8, Catalog #: 127633, Biolegend), F4/80-PE (clone BM8, Catalog #: 123110, Biolegend), CD64-BV421 (clone X54-5/7.1, Catalog #: 139309, Biolegend), IFNGR1/CD119-APC (Clone: REA189, Catalog #: 130-132-427, Miltenyi Biotec). For the analyses in Figure 5M and Figure S14D, the antibody panel included CD45-Alexa Fluor 700 (clone 30-F11, Catalog #: 103128, Biolegend), CD11b-BV650 (clone M1/70, Catalog #: 101259, Biolegend), Ly6G-BV510 (clone 1A8, Catalog #: 127633, Biolegend), F4/80-PE (clone BM8, Catalog #: 123110, Biolegend), CD64-BV421 (clone X54-5/7.1, Catalog #: 139309, Biolegend), Phospho-Stat1 (Tyr701)-APC (Clone: Stat1Y701-3E6, Catalog #: MA5-37041, Invitrogen). Live cells were identified as those not stained with the Zombie viability dye (Biolegend). Flow cytometric analysis was performed using Beckman Coulter's CytoFlex LX. The acquired data were analyzed with FlowJo software (Tree Star) and reported as cell numbers per heart tissue. Cell sorting was conducted using a BD FACS Aria II instrument. The following antibodies were used: CD45-Alexa Fluor 700 (clone 30-F11, Catalog #: 103128, Biolegend), CD11b-BV650 (clone M1/70, Catalog #: 101259, Biolegend), Ly6G-FITC (clone 1A8, Catalog #: 11-9668-82, eBioscience), F4/80-BV421 (clone BM8, Catalog #: 123137, Biolegend), MHC-II-PE (clone M5/114.15.2, Catalog #: 107607, Biolegend), CD11c-BV605 (clone N418, Catalog #:117334, Biolegend), CD3-BV510 (clone 145-2C11, Catalog #: 100353, Biolegend), CD19-PE-CY7 (clone 6D5, Catalog #: 115519, Biolegend), NK1.1-APC (clone S17016D, Catalog #: 156505, Biolegend) (Figure S4). CD45-Alexa Fluor 700 (clone 30-F11, Catalog #: 103128, Biolegend), CD11b-BV650 (clone M1/70, Catalog #: 101259, Biolegend), Ly6G-BV510 (clone 1A8, Catalog #: 127633, Biolegend), F4/80-PE (clone BM8, Catalog #: 123110, Biolegend), CD64-BV421 (clone X54-5/7.1, Catalog #: 139309, Biolegend), MHC-II-FITC (clone M5/114.15.2, Catalog #: 107605, Biolegend), CCR2-Alexa Fluor 647 (clone Y15-488.rMAb, Catalog #: 568347, BD) (Figure S5). CD45-Alexa Fluor 700 (clone 30-F11, Catalog #: 103128, Biolegend), CD11b-BV650 (clone M1/70, Catalog #: 101259, Biolegend), Ly6G-BV510 (clone 1A8, Catalog #: 127633, Biolegend), F4/80-PE (clone BM8, Catalog #: 123110, Biolegend), CD64-BV421 (clone X54-5/7.1, Catalog #: 139309, Biolegend) (Figure 4C, Figure 7G, Figure S8C, Figure S10C, and Figure S15C).

Peripheral blood (PB) cells were collected from the retro-orbital vein. Red blood cells were lysed using 1X RBC Lysis Buffer followed by incubation with the Fc blocker. Antibodies were then incubated with the cells for 20 minutes at room temperature in the dark. The antibody panel used for PB flow cytometric analyses consisted of CD45.1-APC (clone A20, Catalog #: 17-0453-82, eBioscience) and CD45.2-FITC (clone 104, Catalog #: 11-0454-82, eBioscience) (Figure 2F). Data acquisition was conducted using Beckman Coulter's CytoFlex LX, and the acquired data were further processed and analyzed with FlowJo Software.

Bone marrow-derived macrophages: Polarized macrophages were examined using antibodies against F4/80-FITC (clone BM8, Catalog #: 11-4801-82, eBioscience) and CD86-PE (clone GL1, Catalog #:12-0862-82, eBioscience) (Figure 8F), followed by flow cytometry analysis.

RNA extraction and quantitative RT-PCR

Total RNA was extracted from sorted macrophages and BMDMs employing the RNeasy Mini Kit (Catalog #: 74104, Qiagen). Total RNA from cardiac tissue was isolated using TRIzol reagent (Catalog #: 15596026, Thermo Fisher Scientific). Subsequently, the Reverse Transcription Kit (Catalog #: 205313, Qiagen) was utilized to synthesize cDNA from mRNA, following the manufacturer's instructions. Reverse transcription was carried out at 42°C for 15 min, followed by an inactivation step at 95°C for 3 min. The resulting cDNA fragments were subjected to amplification in a real-time quantitative PCR machine (Applied Biosystems) using the SYBR Green PCR kit (Catalog #: 208056, Qiagen). The real-time cycler condition was set as follows: an initial activation step at 95ºC for 2 minutes, followed by a 2-step cycling procedure (denaturation at 95ºC for 5 seconds, combined annealing/extension at 60ºC for 10 seconds), repeated for 40 cycles. The mRNA levels of the target genes were normalized to the endogenous GAPDH expression and calculated as relative mRNA expression or fold

change using the $\Delta\Delta C_T$ method. Primer sequences for the genes of interest can be found in Table S11.

Protein preparation and immunoblot analysis

Cultured cells were suspended (myocardial tissues were homogenized) and sonicated in 1x RIPA lysis buffer (Catalog #: ab156034, Abcam) containing protease inhibitors (Catalog #: P8340, Sigma-Aldrich) and phosphatase inhibitors (Catalog #: 04906845001, Roche). Then the lysates were centrifuged, and the supernatants were collected as whole-cell proteins. Pierce BCA assay was performed to determine protein concentrations. Total protein was separated by SDS-PAGE and then transferred to a PVDF membrane. The stacking gel was fixed at 5% acrylamide/bis-acrylamide. The % resolving gel was determined by the predicted molecular weight (MW) of the protein of interest. A 7.5% resolving gel was used for proteins with MW >120kDa. A 10% resolving gel was utilized to resolve proteins within the 50~120kDa range. A 15% resolving gel was used for proteins with MW <50kDa. Primary antibodies used to specifically detect the proteins of interest were as follows: Anti-RNF149 (Catalog #: PA5-110306, Invitrogen), Anti-IFNGR1(Catalog #: MA5-35147, Invitrogen), IL-6 (D5W4V) Rabbit mAb (Catalog #: 12912, CST), NOS2 (D6B6S) Rabbit mAb (Catalog #: 13120, CST), IL-23 p19 Antibody (Catalog #: PA5-20239, Invitrogen), Anti-G-CSF antibody (Catalog #: ab181053, Abcam), Phospho-Stat1 (Tyr701) (58D6) Rabbit mAb (Catalog #: 9167, CST), Stat1 (D1K9Y) Rabbit mAb (Catalog #: 14994, CST), anti-HA (Catalog #: 3724, CST), anti-Flag (Catalog #: F3165, Sigma-Aldrich), anti-Myc (Catalog #: 2278, CST), K48-linkage Specific Polyubiquitin (D9D5) Rabbit mAb (Catalog #: 8081 CST), GAPDH (14C10) Rabbit mAb (Catalog #: 2118, CST). Anti-rabbit IgG, HRP-linked Antibody (Catalog #: 7074, CST) and Anti-mouse IgG, HRP-linked Antibody (Catalog #: 7076, CST) were used to visualize the binding of primary antibodies in combination with the enhanced-chemiluminescent (ECL) substrate (Catalog #: RPN2109, GE). Quantitative analysis of the protein bands was processed with Image J software.

Immunoprecipitation (IP) assay

For immunoprecipitation assays, HEK293T cells harvested 36 h post-transfection, *Rnf149*$^{+/+}$ and *Rnf149*$^{-/-}$ BMDMs with or without IFN-γ (Catalog #: 315-05, PeproTech) stimulation were lysed in 1x RIPA buffer (Catalog #: ab156034, Abcam) supplemented with protease inhibitors (Catalog #: P8340, Sigma-Aldrich). After centrifugation, the collected supernatants were incubated with the specified IP antibodies for 2 h at 4 °C and subsequently pulled down using protein A/G Plus-Agarose (Catalog #: sc-2003, Santa Cruz) for 6 h at 4 °C, followed by washing five times with 1x RIPA buffer. After washing, the immunoprecipitated components were eluted through boiling in the immunoblot sample-loading buffer. For the immunoblot analysis, the immunoprecipitates and input lysates were separated via SDS-PAGE, followed by transferring onto PVDF membranes (Millipore) and detected with specific antibodies.

Enzyme-Linked Immunosorbent Assay (ELISA)

The supernatants of muse heart tissue lysates were harvested, and the concentration of IFN-γ was quantified using commercially available ELISA Kits (Catalog #: 900-K98, PeproTech), following the manufacturer's protocol. After the addition of the stop solution, the optical density was measured at 450 nm (ELx800, BioTek Instruments).

Dual-luciferase reporter assay

Plasmid transfection for dual-luciferase reporter assay was conducted as described above. Luciferase activity was assessed using the Dual-Luciferase Reporter Assay System (Catalog #: E1910, Promega) following the guidelines provided by the manufacturer. In brief, cells were collected in a passive lysis buffer, and the activities of firefly and renilla luciferase in the lysate were quantified using a GloMax 20/20 Luminometer (Promega). Renilla luciferase activity (pRL-TK) served as an internal control due to variations in transfection efficiency. The luciferase activity of firefly was normalized to that of renilla in order to determine the promoter activity. The results were expressed as fold changes compared to the empty vector group.

Chromatin immunoprecipitation (ChIP) assay

The ChIP assay was conducted employing a commercially available chromatin IP Kit (Millipore), following the manufacturer's instructions. Briefly, cells were subjected to 1% formaldehyde for 10 min at room temperature to facilitate the cross-linking of proteins to DNA. The cross-linked chromatin was subsequently fragmented into DNA segments of 200-1000 bp using sonication. The sonicated cross-linked chromatin was used for immunoprecipitation with a specific STAT1 antibody (Catalog #: 14994, CST) or a normal rabbit IgG antibody as a negative control. The immunoprecipitated complex was then collected using Protein G magnetic beads. Following this, the immunoprecipitated chromatin was eluted from the antibody/Protein G magnetic beads followed by reversal of cross-links and purification utilizing a spin column (Catalog #: 14209, CST). The purified immunoprecipitated DNA was amplified by qPCR utilizing specific primers designed for the *Rnf149* gene promoter. The results were presented as a percent of the total input DNA, and the primer sequences employed for ChIP-qPCR can be found in Figure S16.

Transcriptome

Transcriptome sequencing for heart tissue samples was conducted by OE Biotech Co., Ltd. (Shanghai, China). The sample size for the transcriptome study was calculated using RNASeqPower_1.42.0 in R, with a coefficient of variation (CV) of 0.1, an effect size of 2, α of 0.05, and a statistical power of 80%, indicating a minimum requirement of 4 mice per group. Total RNA was extracted using the TRIzol reagent (Invitrogen) according to the manufacturer's protocol. RNA purity and quantification were evaluated using the NanoDrop 2000 spectrophotometer. RNA integrity was assessed using the Agilent 2100 Bioanalyzer. The libraries were constructed using VAHTS Universal V6 RNA-seq Library Prep Kit (Vazyme) according to the manufacturer's instructions. The libraries were sequenced on an Illumina Novaseq 6000 platform, and 150 bp paired-end reads were generated. FPKM of each gene was calculated, and the read counts of each gene were obtained by HTSeq-count. Raw reads ranging from 47.12 to 50.93 M were generated for each sample. The raw reads, in fastq format, were firstly processed using fastp to eliminate low-quality reads, resulting in the retention of 46.49 to 50.20 M clean reads per sample for further analysis. The clean reads were then aligned to the reference genome (GRCm39) using HISAT2. Subsequently, the FPKM of each gene was calculated and the read counts of each gene were determined by HTSeq-count. A total of 17,734 genes were used for subsequent analyses. Principal component analysis (PCA) was performed using R (v 3.2.0) to evaluate the biological duplication of samples. Differentially expressed genes (DEGs) were identified using the R package DESeq2. The *P*-value for each gene was calculated using the negative binomial (NB) distribution test. Absolute fold change in gene expression≥2 and *P*-value<0.05 were set as the thresholds for significantly differential expression genes. Hierarchical cluster analysis of DEGs was performed using R (v 3.2.0) to demonstrate the expression pattern of genes in different groups and samples. KEGG pathway enrichment analysis of DEGs was performed using R based on the hypergeometric distribution test. The raw data for transcriptome sequencing have been deposited in the NCBI Sequence Read Archive (accession ID: PRJNA1102525).

Bioinformatic analysis of external datasets

STAT1 ChIP-seq data pertaining to BMDMs were sourced from the NCBI Gene Expression Omnibus (Accession ID: GSE84520) and analyzed in the Cistrome platform. Enriched peaks for target genes were then visualized within the UCSC genome browser. The enriched DNA motifs at the STAT1 binding sites were discerned via Cistrome SeqPos motif analysis, and the resulting motif logos (z-score=-23.751; *P*-value=8.364E-70) were presented in Figure 8A. Protein interactome for RNF149 was acquired from the BioGRID database, and KEGG enrichment analysis of potential interacting proteins was performed utilizing the online analysis tool DAVID (Database for Annotation, Visualization, and Integrated Discovery)[20]. Transcriptome data in Figure S1 were taken from the NCBI Gene Expression Omnibus

(Accession ID: GSE115354, GSE126772), and the analysis of gene expression profiles was conducted using DESeq2 in R (v 3.2.0).

Statistics

Statistical analysis was performed following the Statistical Reporting Recommendations of *Circulation Research*. All presented values are denoted as mean ± SEM. The number of samples is detailed in the individual Figure legends and represents biological replicates, not technical replicates. The analysis of all raw data and results was conducted in a blinded manner. Quantification of gene expression was reported relative to the control group within each experiment, i.e., Figure 3C (WT sham), Figure 4C (WT cardiac MΦ), Figure 7G (WT+NC MΦ), Figure S8C (AAV-F4/80-NC), Figure S10C (Adnull), Figure S13 (WT-MI), Figure S14A (Day 0), Figure S15B (AAV-F4/80-NC), and Figure S15C (WT+NC MΦ). The representative image for each group was chosen based on the mean value. Statistical analysis was executed employing GraphPad PRISM 9.0 software. The Shapiro-Wilk test was used to determine the normality of data before applying parametric or non-parametric tests. For *in vitro* experiments (Figure 5L, 8C, 8D, 8E, 8F, 8H, and Figure S15B), as each experimental dataset represented an average of a large number of cultured cells, we assumed the data was normally distributed based on the central limit theorem. For *in vivo* experiments, the echocardiographic data (Figure 2B, 2H, 7D, and Figure S8D, S9E, S10D) ($6 \leqslant n < 10$) passed the Shapiro-Wilk test. For normally distributed data, statistical analysis was employed utilizing parametric tests including unpaired and two-tailed t-test (for two groups of data), one-way ANOVA with adjustment for multiple comparisons using Bonferroni's or Dunnett's post hoc test (for three or more groups of data), and two-way ANOVA with Bonferroni's multiple comparisons test (for multiple group comparisons with two mutually exclusive variables). Additionally, for data that required repeated measurements for an individual, two-way repeated-measures ANOVA analysis with Bonferroni's post hoc test was utilized for pairwise comparisons within groups. For non-normally distributed data or in cases where the sample size for *in vivo* experiments was insufficient to test normality (i.e., n=5 per group) (Figure 1C, 1E, 1H, 1I, 5K, and Figure S3, S8C, S10C, S14D, S15C), non-parametric tests including Mann-Whitney test (for two groups comparison) or Kruskal-Wallis test with Dunn's post hoc test (for multiple groups comparison) were employed. Detailed statistical methods are provided in the corresponding figure legends. Differences were considered statistically significant at P-value<0.05.

Supplemental Figures

Figure S1

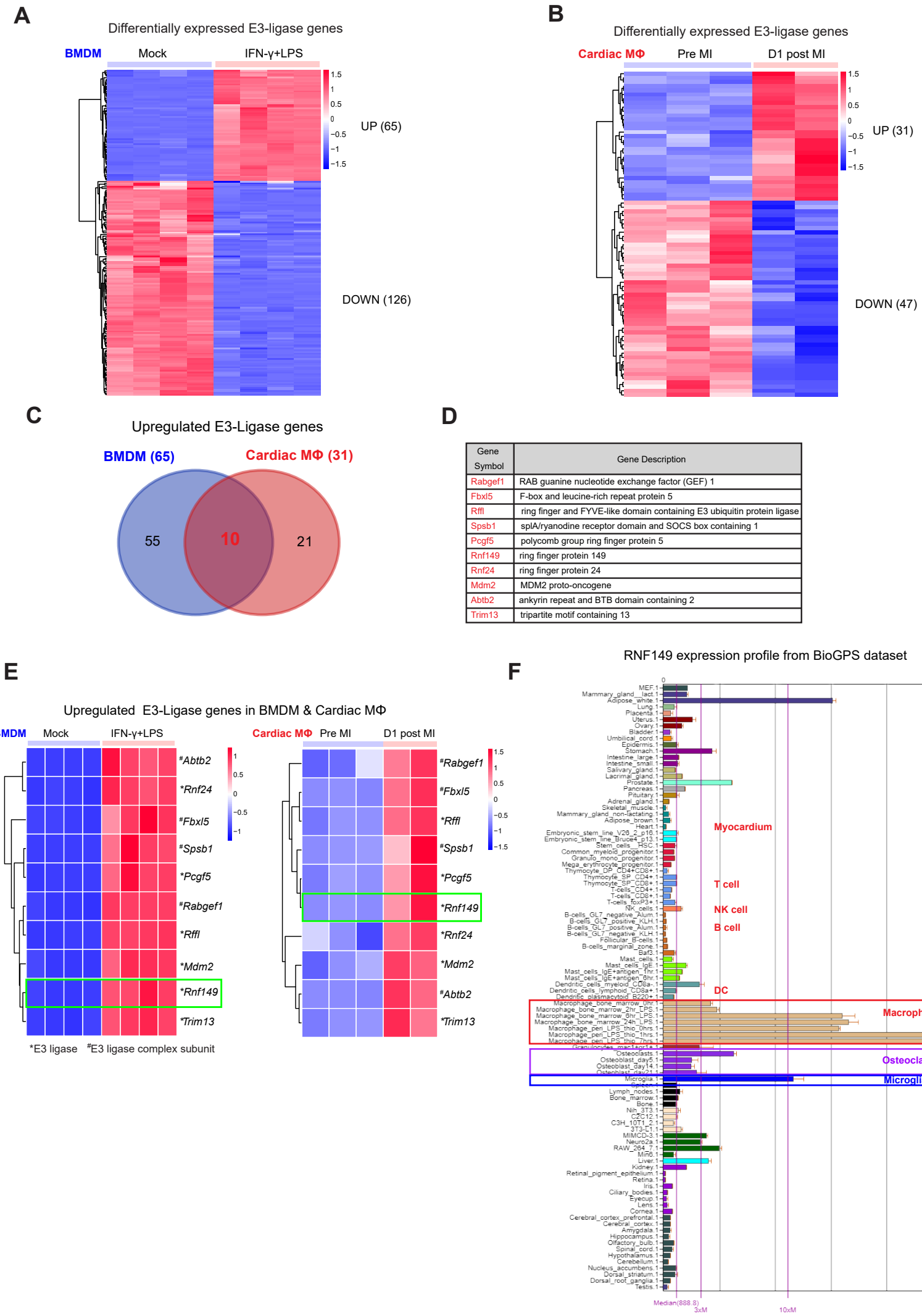

Gene Symbol	Gene Description
Rabgef1	RAB guanine nucleotide exchange factor (GEF) 1
Fbxl5	F-box and leucine-rich repeat protein 5
Rffl	ring finger and FYVE-like domain containing E3 ubiquitin protein ligase
Spsb1	splA/ryanodine receptor domain and SOCS box containing 1
Pcgf5	polycomb group ring finger protein 5
Rnf149	ring finger protein 149
Rnf24	ring finger protein 24
Mdm2	MDM2 proto-oncogene
Abtb2	ankyrin repeat and BTB domain containing 2
Trim13	tripartite motif containing 13

Figure S1. Expression alteration of E3 ligase genes in macrophages subjected to inflammatory stimuli. A, Heatmap illustrating differentially expressed E3 ligase genes, including 65 upregulated (red) and 126 downregulated (blue) gene hubs in bone marrow-derived macrophages (BMDMs) after IFN-γ/LPS stimulation for 4h; Genes with absolute fold change ≥2 and *P*-value <0.05 are defined as differentially expressed genes, n=4 biological replicates per group (source data obtained from publicly available GEO dataset, GSE115354). **B,** Heatmap depicting the altered expression profiles of E3 ligase genes, including 31 upregulated (red) and 47 downregulated (blue) gene hubs within cardiac macrophages on day 1 after MI; Genes with absolute fold change ≥2 and *P*-value <0.05 are defined as differentially expressed genes, n=3 for baseline and 2 for MI (source data obtained from GEO dataset, GSE126772). **C,** Venn diagram showing intersections of upregulated E3 ligase genes in BMDMs subjected to IFN-γ/LPS stimulation and cardiac macrophages after MI. **D,** The list of 10 upregulated E3 ligase genes obtained from **C. E,** Heatmap illustrating the 10 E3 ligase genes upregulated in both BMDMs with IFN-γ/LPS stimulation and cardiac macrophages after MI. **F,** RNF149 expression profile from BioGPS dataset.

Figure S2

Expression profile from BioGPS dataset

Rabgef1

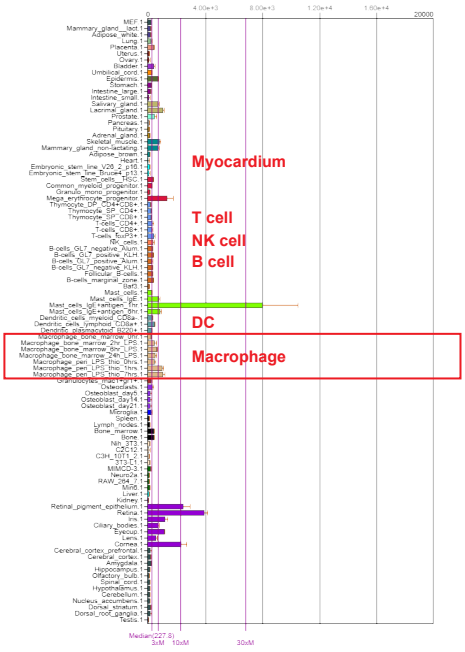

Spsb1

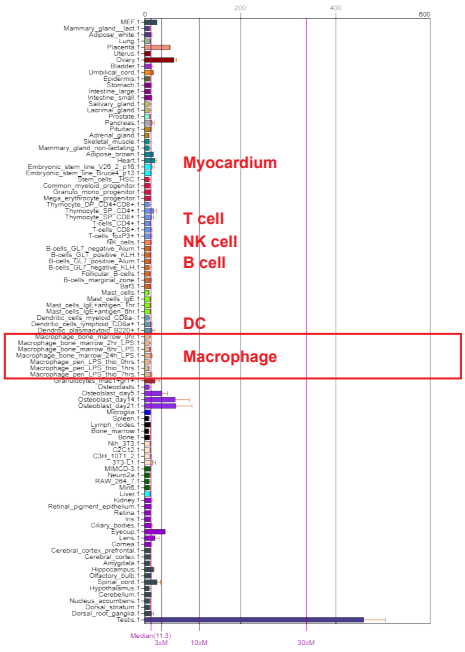

RNF24

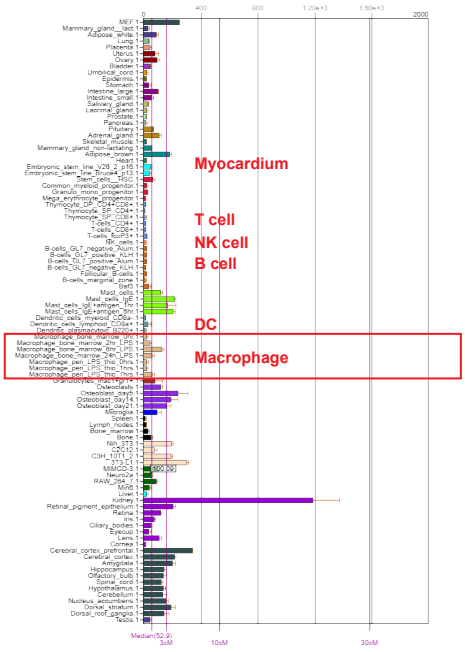

Rffl

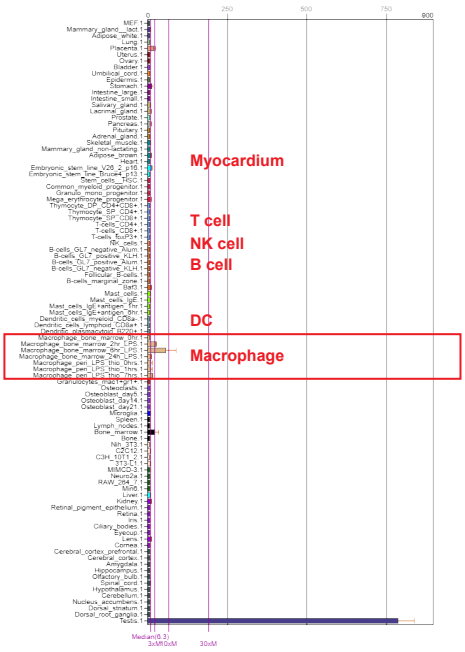

Abtb2

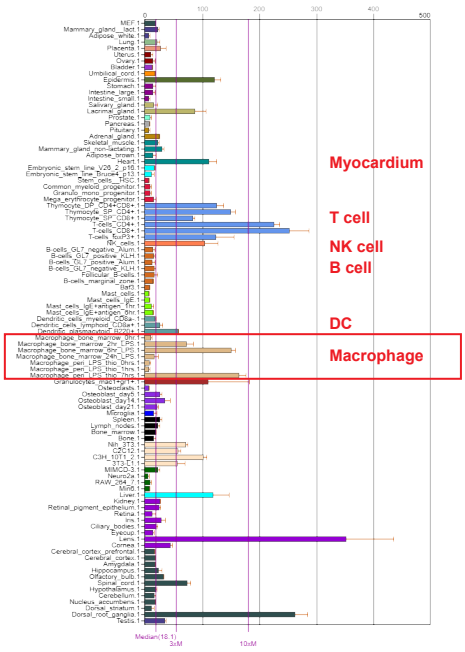

MDM2

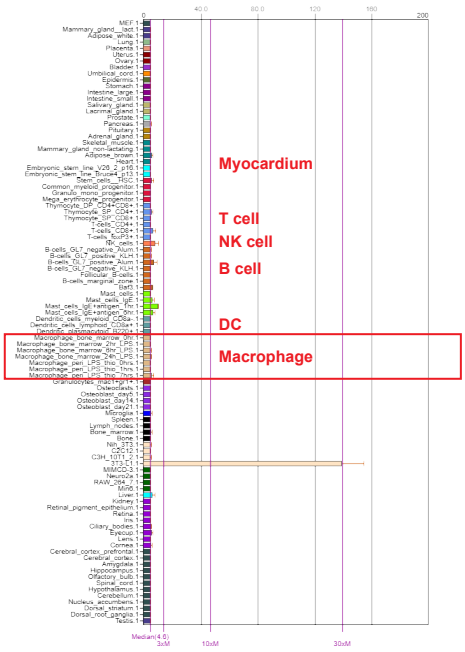

Fbxl5

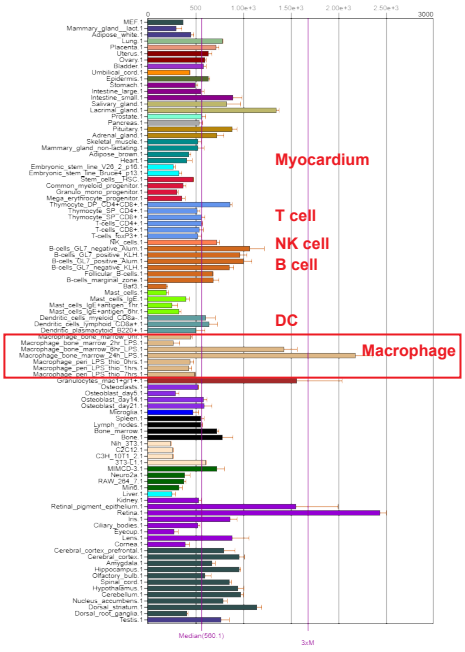

Pcgf5

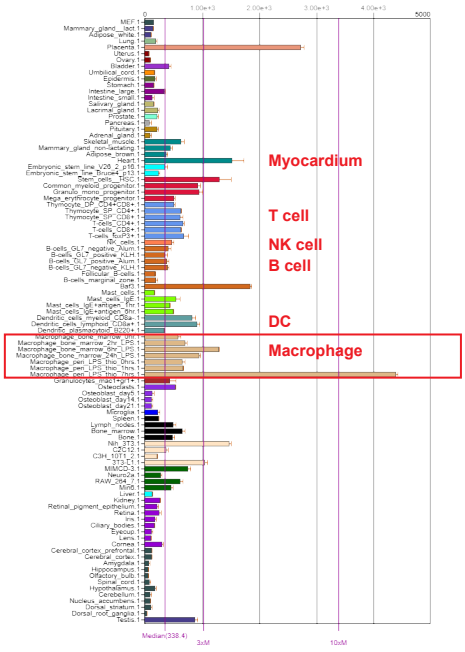

Trim13

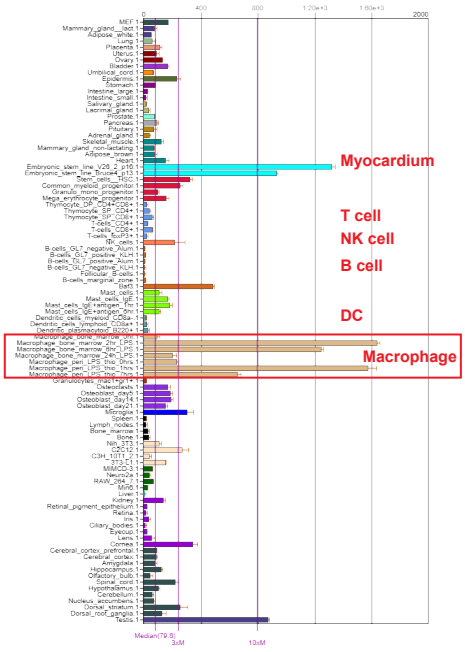

Figure S2. Expression profile of E3 ligase genes *Rabgef1, Spsb1, RNF24, Rffl, Abtb2, MDM2, Fbxl5, Pcgf5,* and *Trim13* derived from the BioGPS dataset.

Figure S3

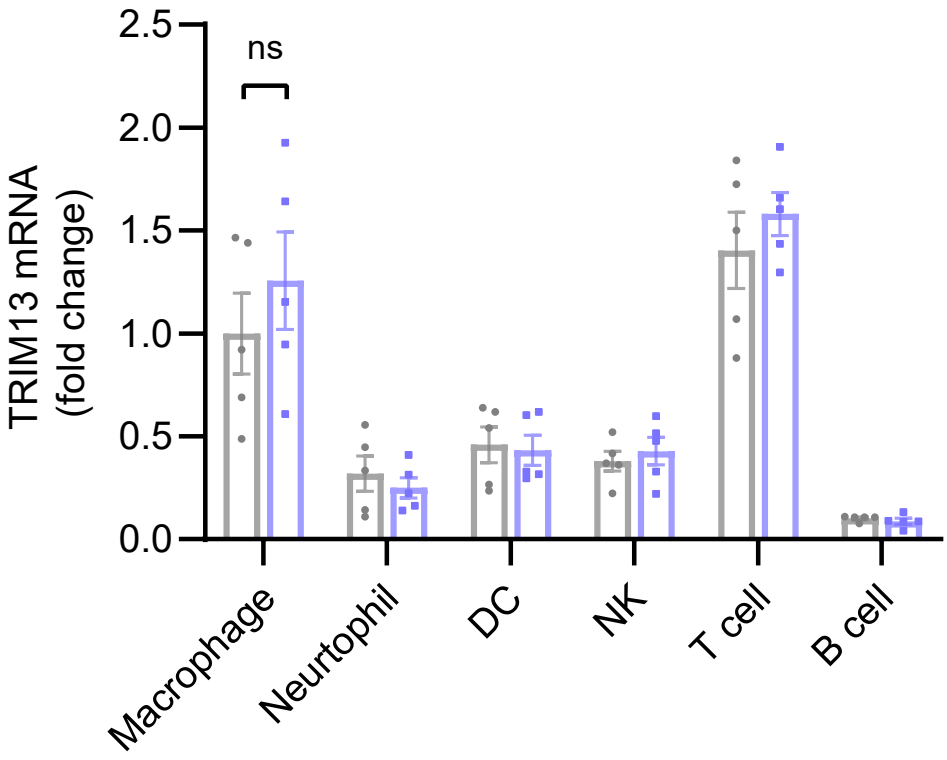
TRIM13 mRNA
(fold change)
2.5
2.0
1.5
1.0
0.5
0.0
ns
Macrophage
Neurtophil
DC
NK
T cell
B cell

Figure S3. Analysis of Trim13 mRNA expression in leukocyte population isolated from WT hearts before and after MI. Data were analyzed using the Kruskal-Wallis test with Dunn's multiple comparisons (n=5).

Figure S4

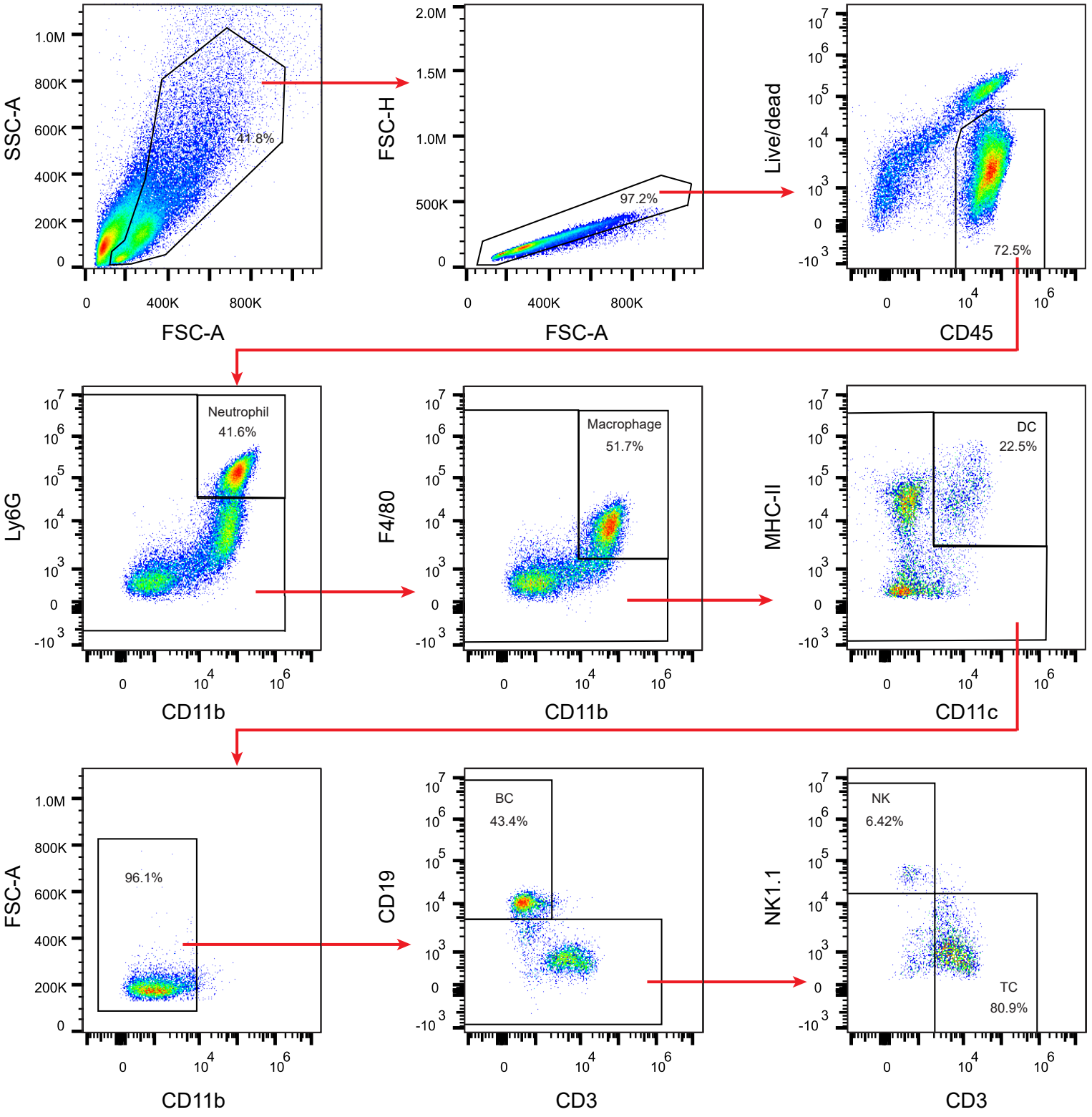
SSC-A
FSC-A
41.8%
FSC-H
FSC-A
97.2%
Live/dead
CD45
72.5%
Ly6G
CD11b
Neutrophil
41.6%
F4/80
CD11b
Macrophage
51.7%
MHC-II
CD11c
DC
22.5%
FSC-A
CD11b
96.1%
CD19
CD3
BC
43.4%
NK1.1
CD3
NK
6.42%
TC
80.9%

Figure S4. Flow cytometry gating strategy for identification of infiltrating immune cells in the infarcted hearts. $CD45^+$ leukocytes were divided into neutrophils ($CD45^+$ $CD11b^+$ $Ly6G^+$), macrophages ($CD45^+$ $CD11b^+$ $Ly6G^-$ $F4/80^+$), dendritic cells (DC) ($CD45^+$ $Ly6G^-$ $F4/80^-$ $MHC\text{-}II^+$ $CD11c^+$), B cells ($CD45^+$ $CD11b^-$ $Ly6G^-$ $F4/80^-$ $MHC\text{-}II^-$ $CD11c^-$ $CD3^-$ $CD19^+$), T cells ($CD45^+$ $CD11b^-$ $Ly6G^-$ $F4/80^-$ $MHC\text{-}II^-$ $CD11c^-$ $CD19^-$ $NK1.1^-$ $CD3^+$) and natural killer (NK) cells ($CD45^+$ $CD11b^-$ $Ly6G^-$ $F4/80^-$ $MHC\text{-}II^-$ $CD11c^-$ $CD19^-$ $CD3^-$ $NK1.1^+$) and harvested for subsequent experiments.

Figure S5

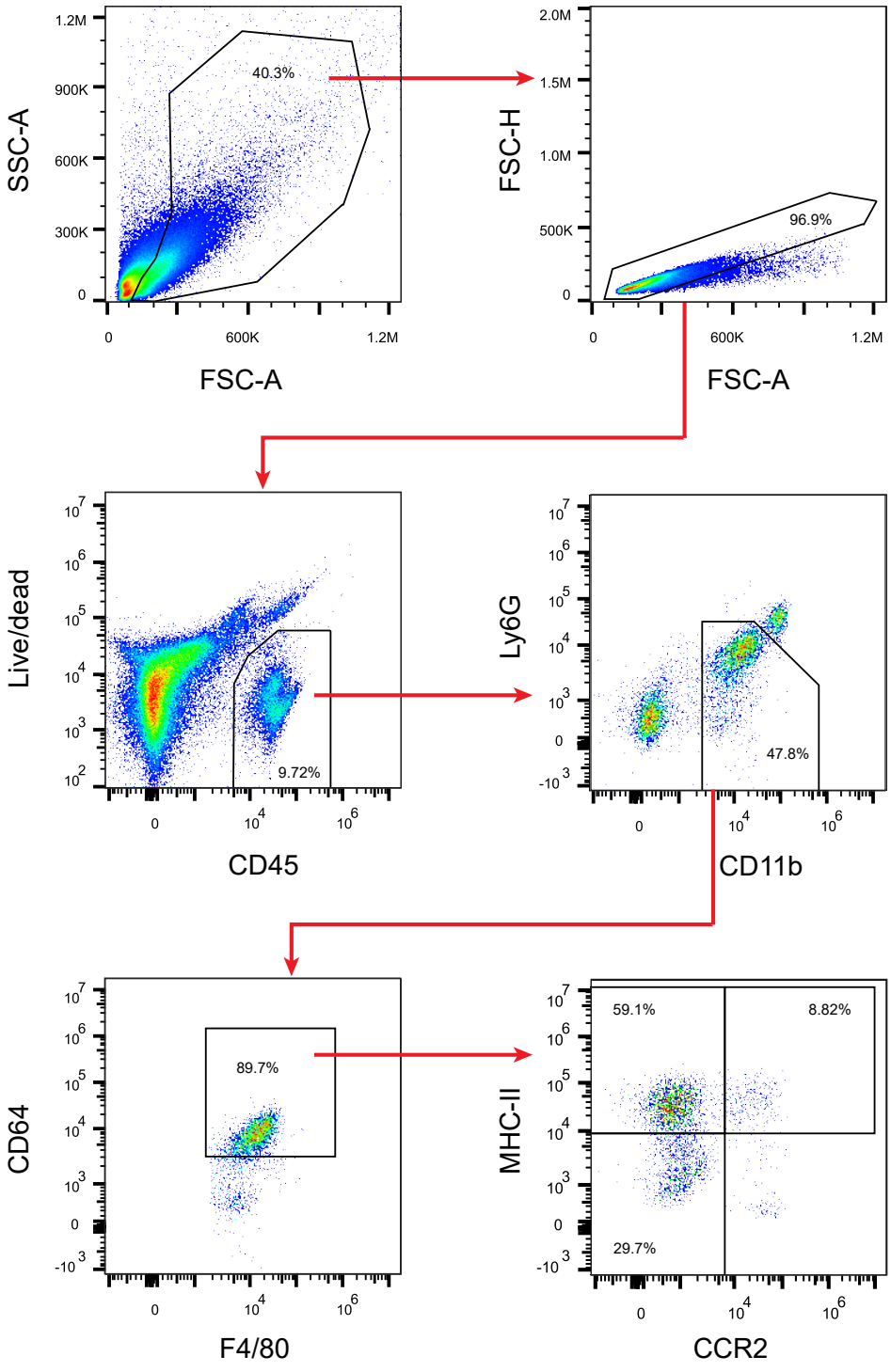
SSC-A
FSC-A
40.3%
FSC-H
FSC-A
96.9%
Live/dead
CD45
9.72%
Ly6G
CD11b
47.8%
CD64
F4/80
89.7%
MHC-II
CCR2
59.1%
8.82%
29.7%

Figure S5. Gating strategy for the identification of macrophage subsets isolated from mouse hearts. Representative flow cytometric dot plots to determine macrophage subsets in mouse hearts at baseline. $CD45^{+}CD11b^{+}Ly6G^{-}F4/80^{+}CD64^{+}$ macrophages were further divided into $CCR2^{-}MHC\text{-}II^{low}$, $CCR2^{-}MHC\text{-}II^{high}$, $CCR2^{+}MHC\text{-}II^{high}$ subsets and harvested for subsequent experiments.

Figure S6

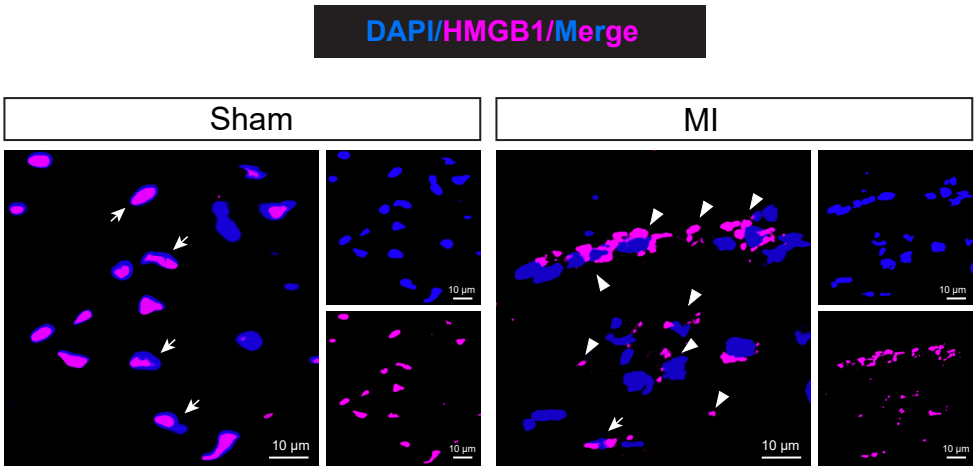

Figure S6. HMGB1 expression in WT mice before and 1 day after MI. Immunofluorescence staining revealed nuclear localization of HMGB1 in WT mice before MI. In contrast, extranuclear HMGB1 staining was observed in the infarcted hearts. HMGB1-positive nuclei are indicated by arrows, while extranuclear staining is marked by arrowheads.

Figure S7

A

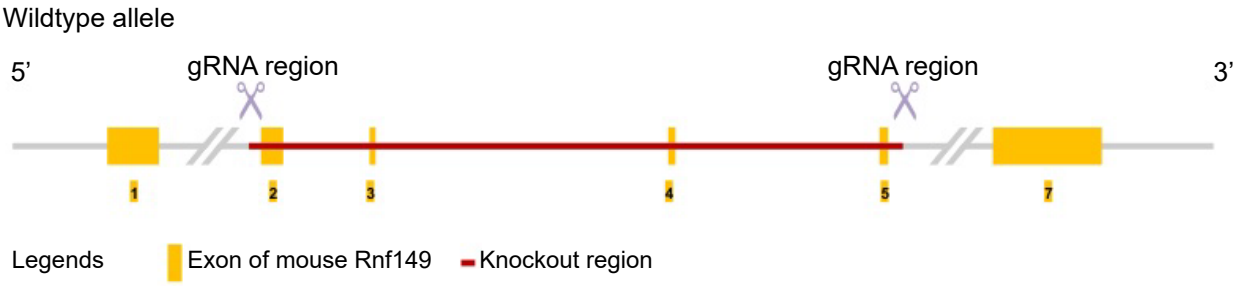

B

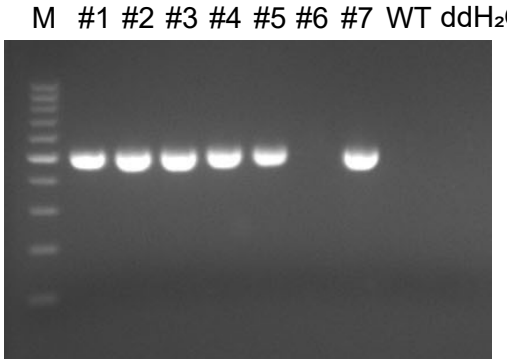

PCR Primer pairs 1:
F1: 5'-TAGTGATCACAGAAGAGCTCTCACA-3'
R1: 5'-AGTGGAAAAGCTGGTTTAGAATCAC-3'
Product size: 502 bp

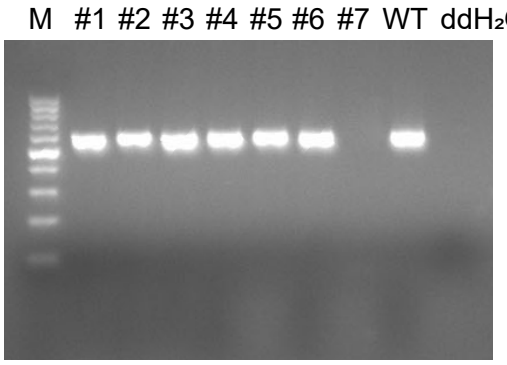

PCR Primer pairs 2:
F1: 5'-TAGTGATCACAGAAGAGCTCTCACA-3'
R2: 5'-AGTGAGAAAATCACCAGGAACTGT-3'
Product size: 586 bp

Mouse genotype:
Homozygote (one band with 502 bp, RNF149$^{ko/ko}$): #7
Heterozygote (two bands with 502 bp and 586 bp, RNF149$^{ko/wt}$): #1, #2, #3, #4, #5
Wildtype allele (one band with 586 bp, RNF149$^{wt/wt}$): #6

C

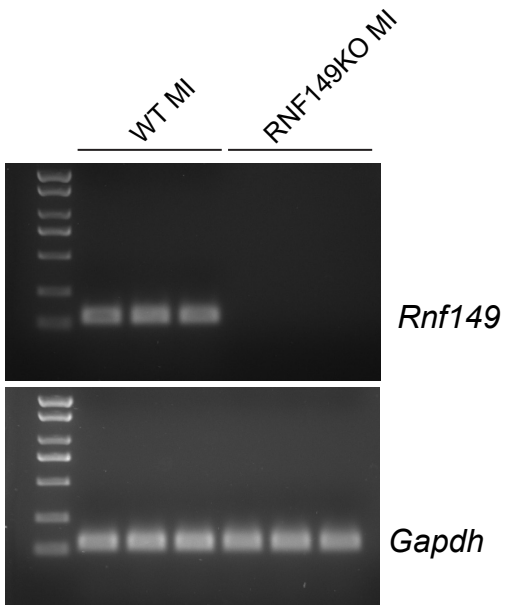

Figure S7. Generation of RNF149 knockout mice. A, Schematic diagram of *Rnf149* knockout strategy. **B,** Representative PCR genotyping of wild-type (+/+), Heterozygote (+/-), and Homozygote (-/-) mice. Sequences of primers used in PCR genotyping are shown. Primer pairs 2 allow amplification of an *Rnf149* fragment (586 bp) in the WT allele whereas primer pairs 1 amplify a mutant allele fragment measuring 502 bp in length. In *Rnf149* Heterozygotes (+/-), both PCR products are generated. **C,** RNF149 mRNA expression levels in MI hearts obtained from RNF149KO and WT littermates.

Figure S8

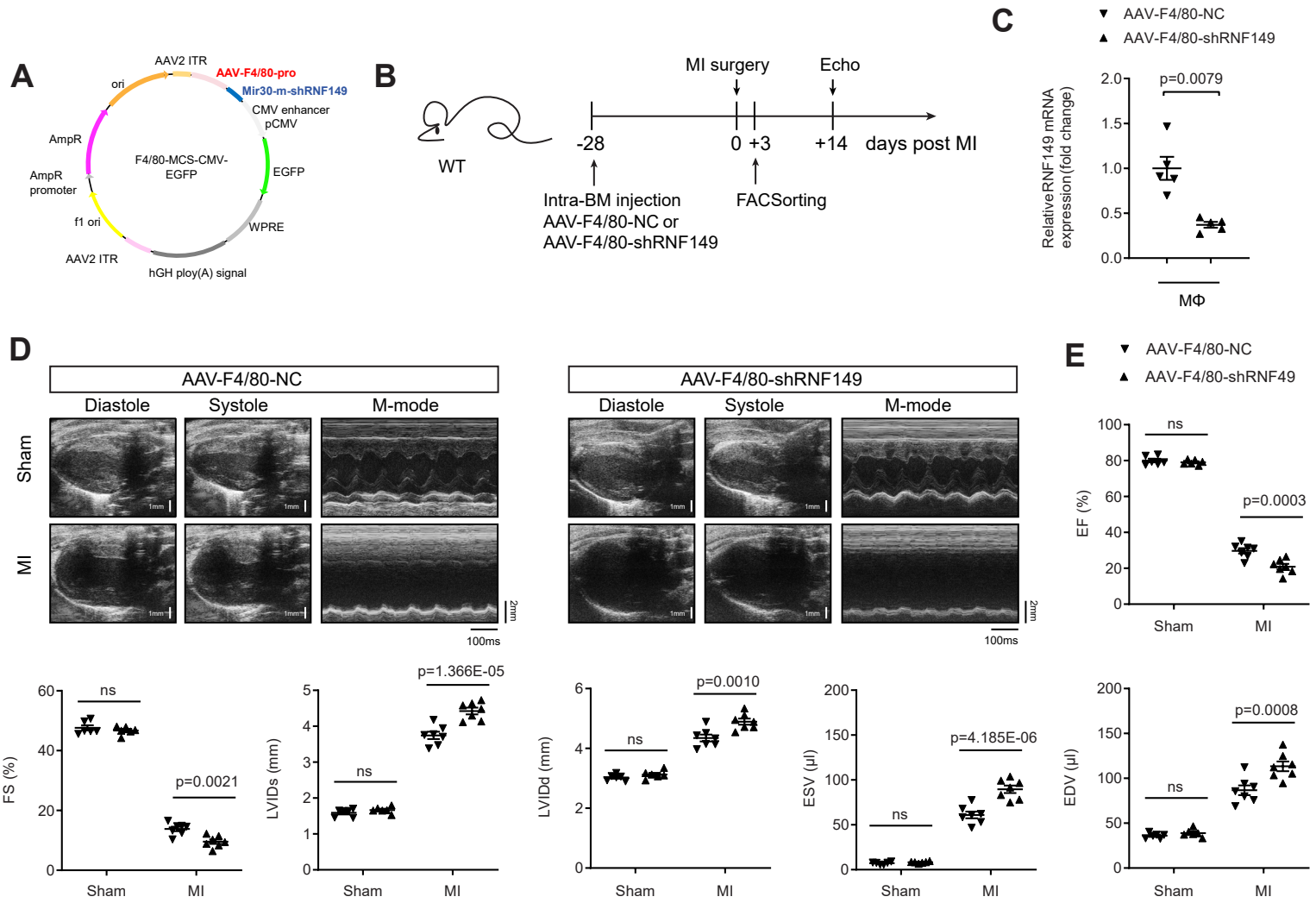
A
AAV2 ITR
AAV-F4/80-pro
Mir30-m-shRNF149
CMV enhancer
pCMV
EGFP
WPRE
hGH ploy(A) signal
AAV2 ITR
f1 ori
AmpR promoter
AmpR
ori
F4/80-MCS-CMV-EGFP
B
WT
MI surgery
Echo
-28
0 +3
+14
days post MI
Intra-BM injection
AAV-F4/80-NC or
AAV-F4/80-shRNF149
FACSorting
C
AAV-F4/80-NC
AAV-F4/80-shRNF149
Relative RNF149 mRNA expression (fold change)
p=0.0079
MΦ
D
AAV-F4/80-NC
AAV-F4/80-shRNF149
Diastole
Systole
M-mode
Sham
MI
100ms
FS (%)
LVIDs (mm)
LVIDd (mm)
ESV (μl)
EDV (μl)
ns
p=0.0021
p=1.366E-05
p=0.0010
p=4.185E-06
p=0.0008
E
AAV-F4/80-NC
AAV-F4/80-shRNF49
EF (%)
p=0.0003

Figure S8. Adeno-associated virus (AAV)-mediated RNF149 knockdown in macrophages exacerbates cardiac dysfunction in mouse models of MI. A, Full sequence map for AAV-F4/80-miR30-m-shRNF149-eGFP (AAV-F4/80-shRNF149); The AAV system harbors a macrophage-specific F4/80 promoter, a miR30-based shRNA targeting RNF149, a cytomegalovirus promoter, and an enhanced GFP reporter. **B,** Design of the RNF149 knockdown study. **C,** mRNA levels of RNF149 in infarct macrophages ($CD45^+CD11b^+Ly6G^-F4/80^+CD64^+$) from the designated groups according to the experimental setup in **B**; n=5 per group. **D-E,** Echocardiographic measurements of LV function in AAV-F4/80-NC and AAV-F4/80-shRNF149 mice after sham operation or 14 days post-MI; n=6 per group for sham and n=7 per group for MI. Data in **C** were analyzed using the Mann-Whitney test. Data in **E** were analyzed using two-way ANOVA with Bonferroni's multiple comparisons test**.** ns, not significant.

Figure S9

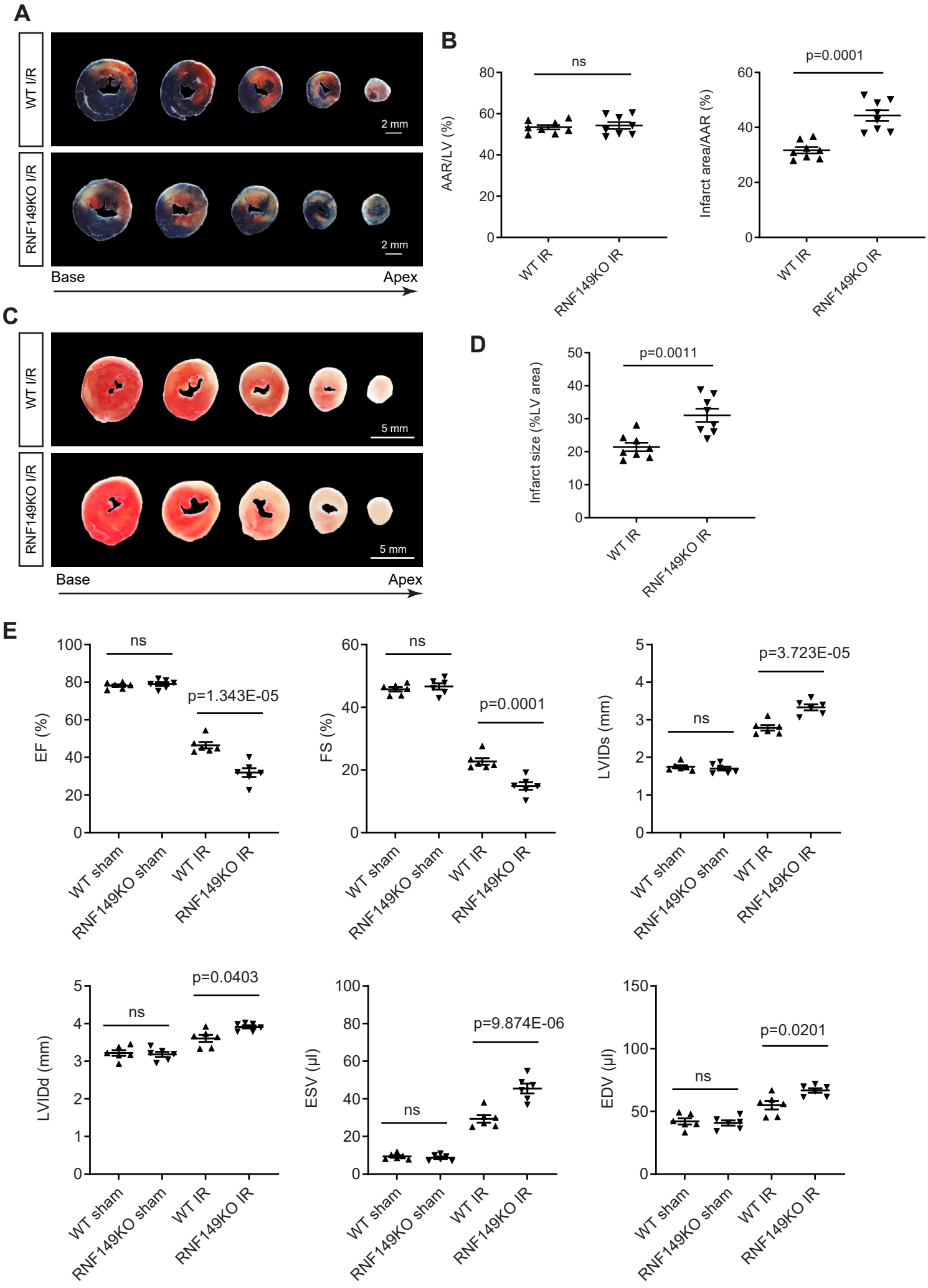
A
WT I/R
RNF149KO I/R
2 mm
2 mm
Base
Apex
B
AAR/LV (%)
ns
WT IR
RNF149KO IR
Infarct area/AAR (%)
p=0.0001
C
WT I/R
RNF149KO I/R
5 mm
5 mm
Base
Apex
D
Infarct size (%LV area)
p=0.0011
E
EF (%)
p=1.343E-05
FS (%)
p=0.0001
LVIDs (mm)
p=3.723E-05
LVIDd (mm)
p=0.0403
ESV (μl)
p=9.874E-06
EDV (μl)
p=0.0201
WT sham
RNF149KO sham
WT IR
RNF149KO IR

Figure S9. RNF149 loss aggravates myocardial IR injury. A, Representative photographs of Evans blue and TTC double stained serial heart slices from WT and RNF149KO mice at day 2 after myocardial IR injury. **B,** Quantitative analysis of infarct size at day 2 post-IR in WT and RNF149KO mice. The ratios of AAR/LV (area at risk/ total left ventricular area) and infarct area/AAR (infarct area/area at risk) were determined, n=8 per group. **C-D,** TTC staining for infarct measurements 2 days after IR in RNF149KO mice compared with WT controls. **E,** Echocardiographic measurements of left ventricular internal diameter at end-systole (LVIDs), left ventricular internal diameter at end-diastole (LVIDd), fractional shortening (FS), ejection fraction (EF), end-diastolic volume (EDV), and end-systolic volume (ESV) in WT and RNF149KO mice at day 4 after IR or the sham surgery; n=6 per group. Data in **B** and **D** were analyzed using unpaired two-tailed student's t-test. Data in **E** were analyzed using two-way ANOVA with Bonferroni's multiple comparisons test**.** ns, not significant.

Figure S10

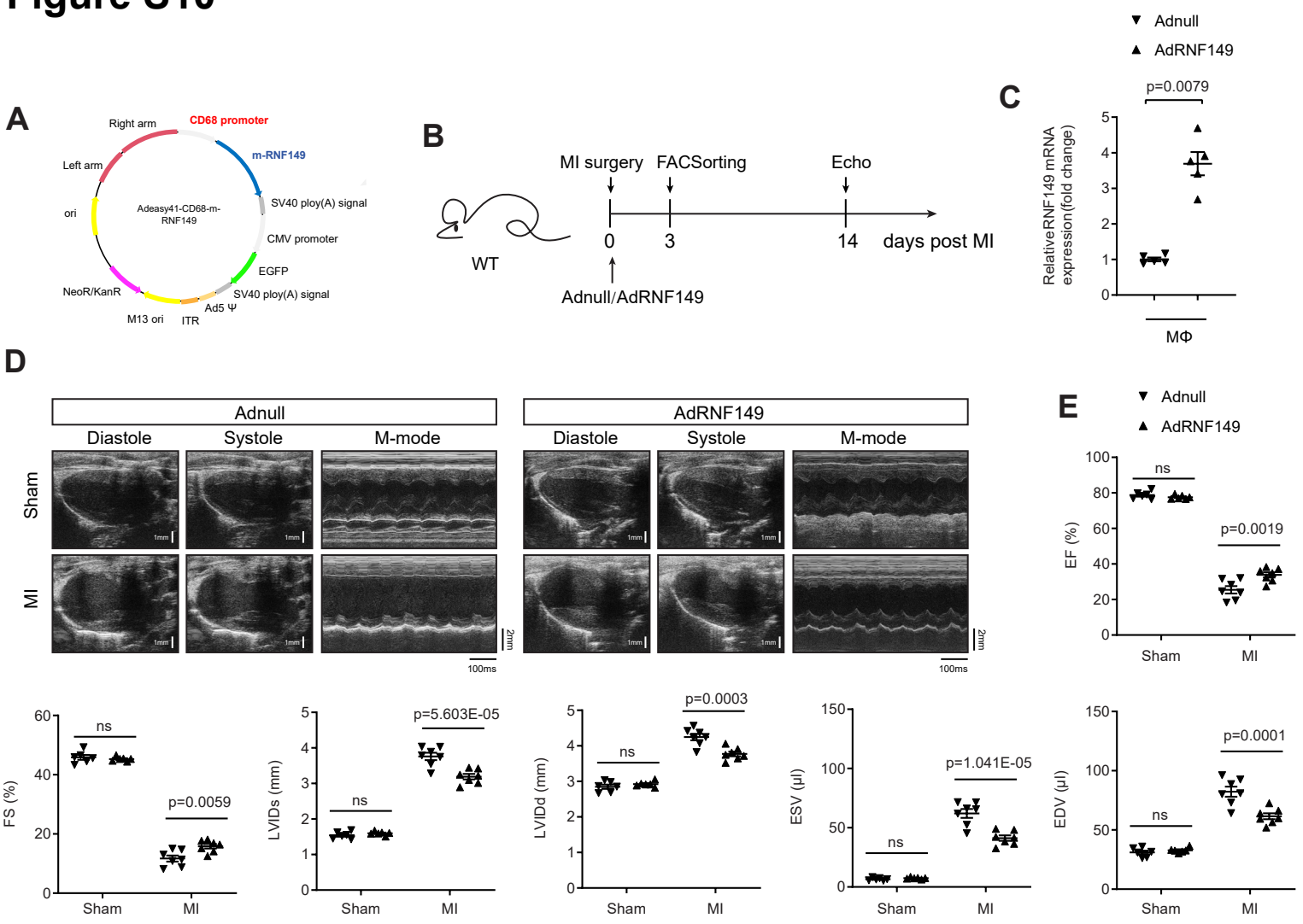
A
Right arm
CD68 promoter
m-RNF149
Left arm
ori
Adeasy41-CD68-m-RNF149
SV40 ploy(A) signal
CMV promoter
EGFP
NeoR/KanR
SV40 ploy(A) signal
Ad5 Ψ
M13 ori
ITR
B
MI surgery
FACSorting
Echo
WT
0
3
14
days post MI
Adnull/AdRNF149
C
Adnull
AdRNF149
p=0.0079
RelativeRNF149 mRNA expression(fold change)
MΦ
D
Adnull
AdRNF149
Diastole
Systole
M-mode
Sham
MI
100ms
E
Adnull
AdRNF149
EF (%)
ns
p=0.0019
FS (%)
p=0.0059
LVIDs (mm)
p=5.603E-05
LVIDd (mm)
p=0.0003
ESV (μl)
p=1.041E-05
EDV (μl)
p=0.0001
Sham
MI

Figure S10. Adenovirus-mediated RNF149 overexpression in macrophages improves cardiac function in mouse models of MI. A, Schematics of adenoviral vector expressing mouse RNF149 driven by CD68 promoter. **B,** Design of the AdRNF149 study. **C,** mRNA levels of RNF149 in infarct macrophages ($CD45^{+}CD11b^{+}Ly6G^{-}F4/80^{+}CD64^{+}$) from the designated groups according to the experimental setup in **B**; n=5 per group. **D-E,** Echocardiographic measurements of LV function in Adnull and AdRNF149 mice after sham operation or 14 days post-MI; n=6 per genotype for sham and n= 7 per genotype for MI. Data in **C** were analyzed using the Mann-Whitney test. Data in **E** were analyzed using two-way ANOVA with Bonferroni's multiple comparisons test**.** ns, not significant.

Figure S11

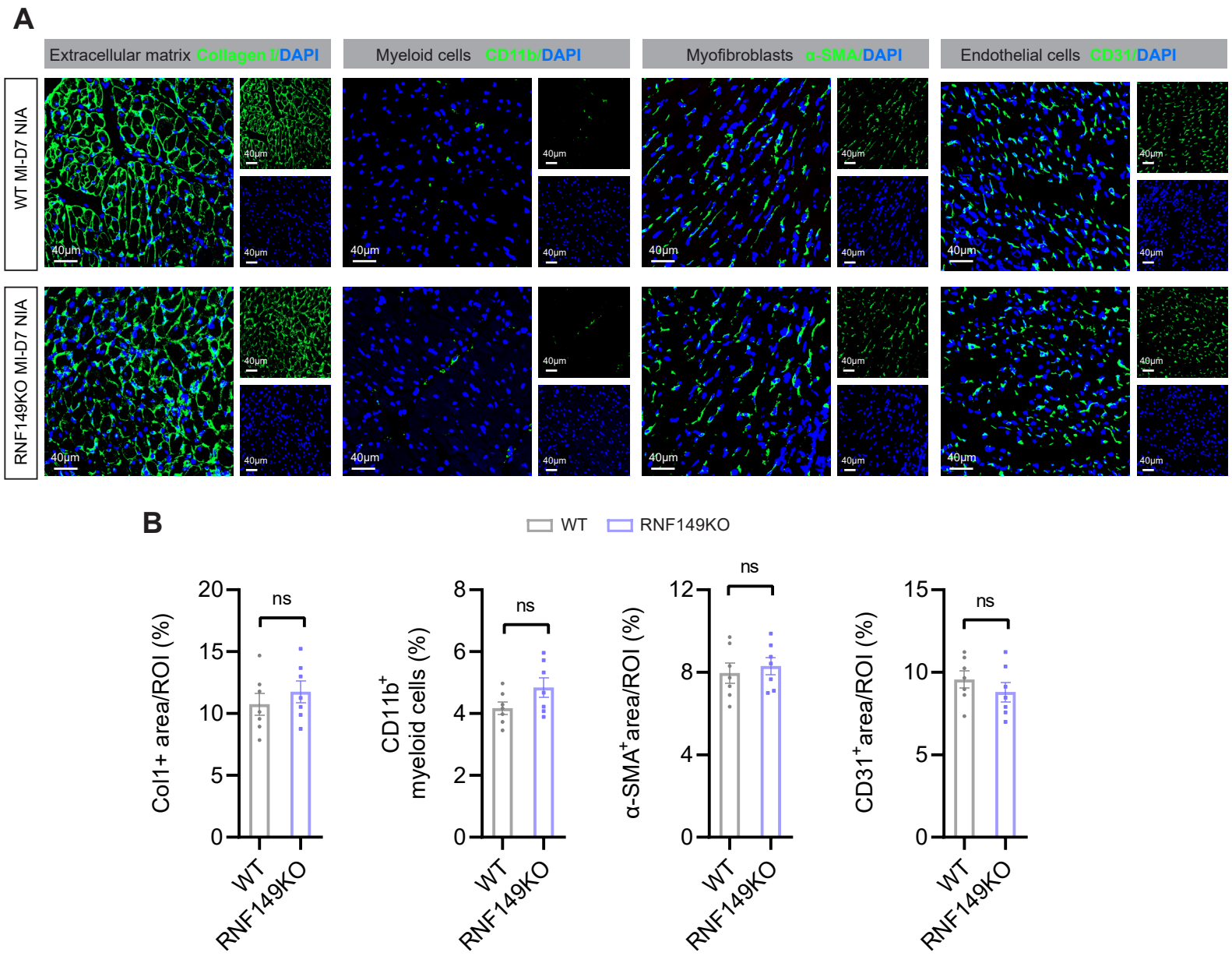
A
Extracellular matrix Collagen I/DAPI
Myeloid cells CD11b/DAPI
Myofibroblasts α-SMA/DAPI
Endothelial cells CD31/DAPI
WT MI-D7 NIA
RNF149KO MI-D7 NIA
40μm
B
WT
RNF149KO
Col1+ area/ROI (%)
CD11b+ myeloid cells (%)
α-SMA+area/ROI (%)
CD31+area/ROI (%)
ns
0
5
10
15
20
2
4
6
8
12

Figure S11. RNF149 deficiency contributes minimally to extracellular matrix remodeling in the non-infarct area. A, Immunofluorescence staining of collagen I, CD11b, α-smooth muscle actin (α-SMA), and CD31 on non-infarct areas of WT and RNF149KO hearts 7 days after MI. **B,** Dot plots showing the quantified data of **A**. n=7 per group. Data were analyzed using unpaired two-tailed student's t-test. ns, not significant.

Figure S12

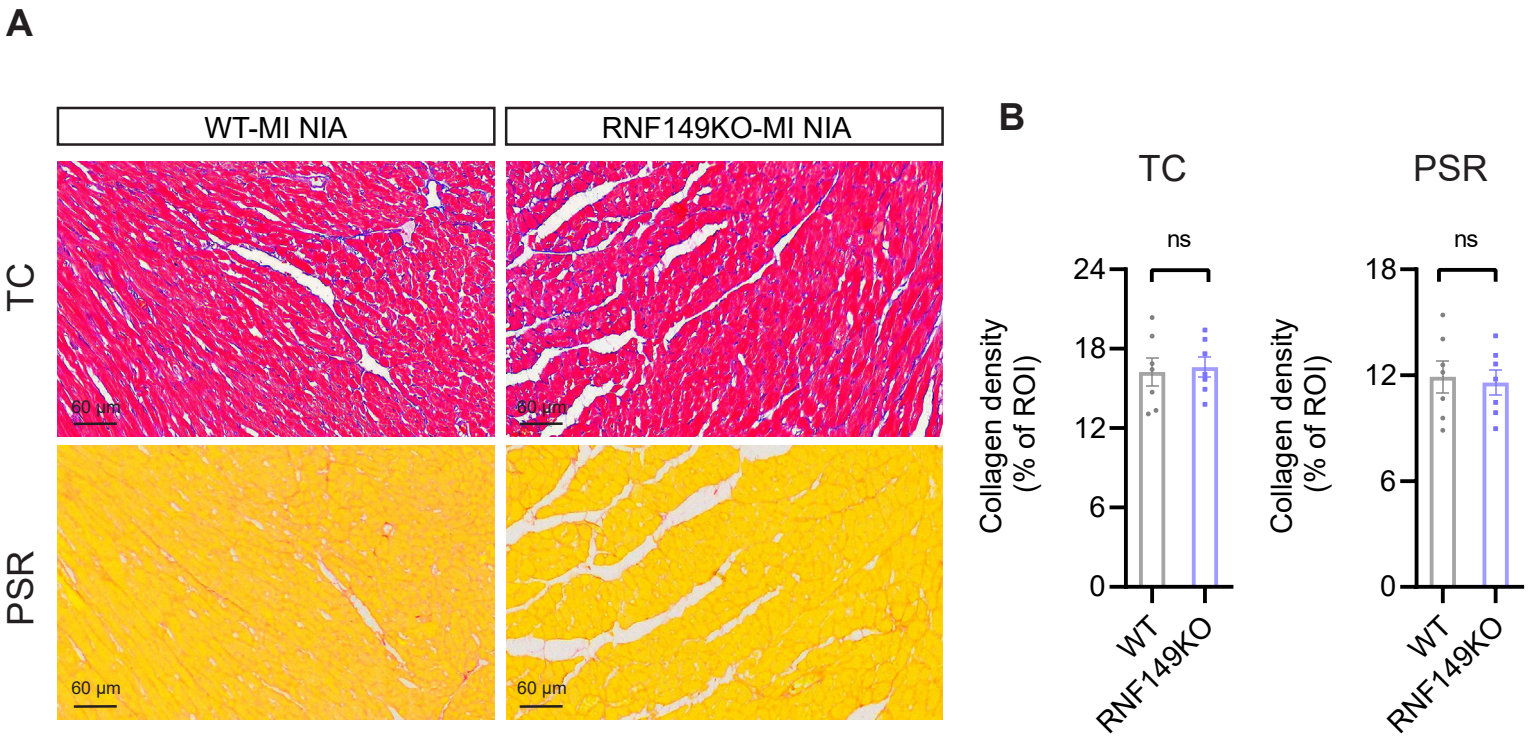
A
WT-MI NIA
RNF149KO-MI NIA
TC
PSR
60 μm
60 μm
60 μm
60 μm
B
TC
PSR
ns
ns
Collagen density (% of ROI)
Collagen density (% of ROI)
24
18
12
6
0
18
12
6
0
WT
RNF149KO
WT
RNF149KO

Figure S12. Comparable collagen content in the non-infarct area of WT and RNF149KO hearts. Masson's trichrome (TC) and Picrosirius red (PSR) staining of heart transverse sections to detect collagen in the non-infarct area of WT and RNF149KO hearts one week after MI (n=7). Data were analyzed using unpaired two-tailed student's t-test. ns, not significant.

Figure S13

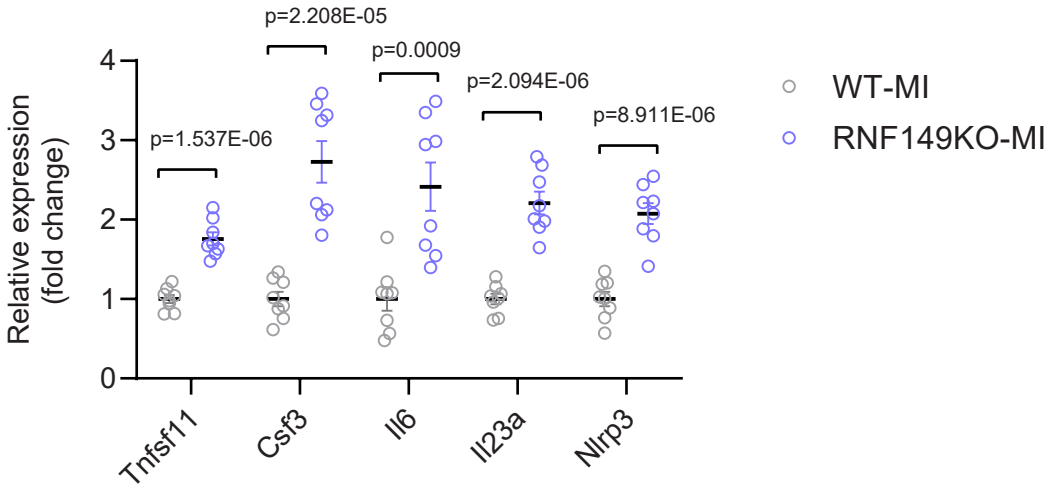
p=2.208E-05
p=0.0009
p=2.094E-06
p=8.911E-06
p=1.537E-06
Relative expression
(fold change)
4
3
2
1
0
Tnfsf11
Csf3
Il6
Il23a
Nlrp3
WT-MI
RNF149KO-MI

Figure S13. *Csf3, IL-6, IL-23a, Nlrp3,* and *Tnfsf11* mRNA expression in WT and RNF149KO hearts 3 days post-MI. n=8 per group. Data were analyzed using unpaired two-tailed student's t-test.

Figure S14

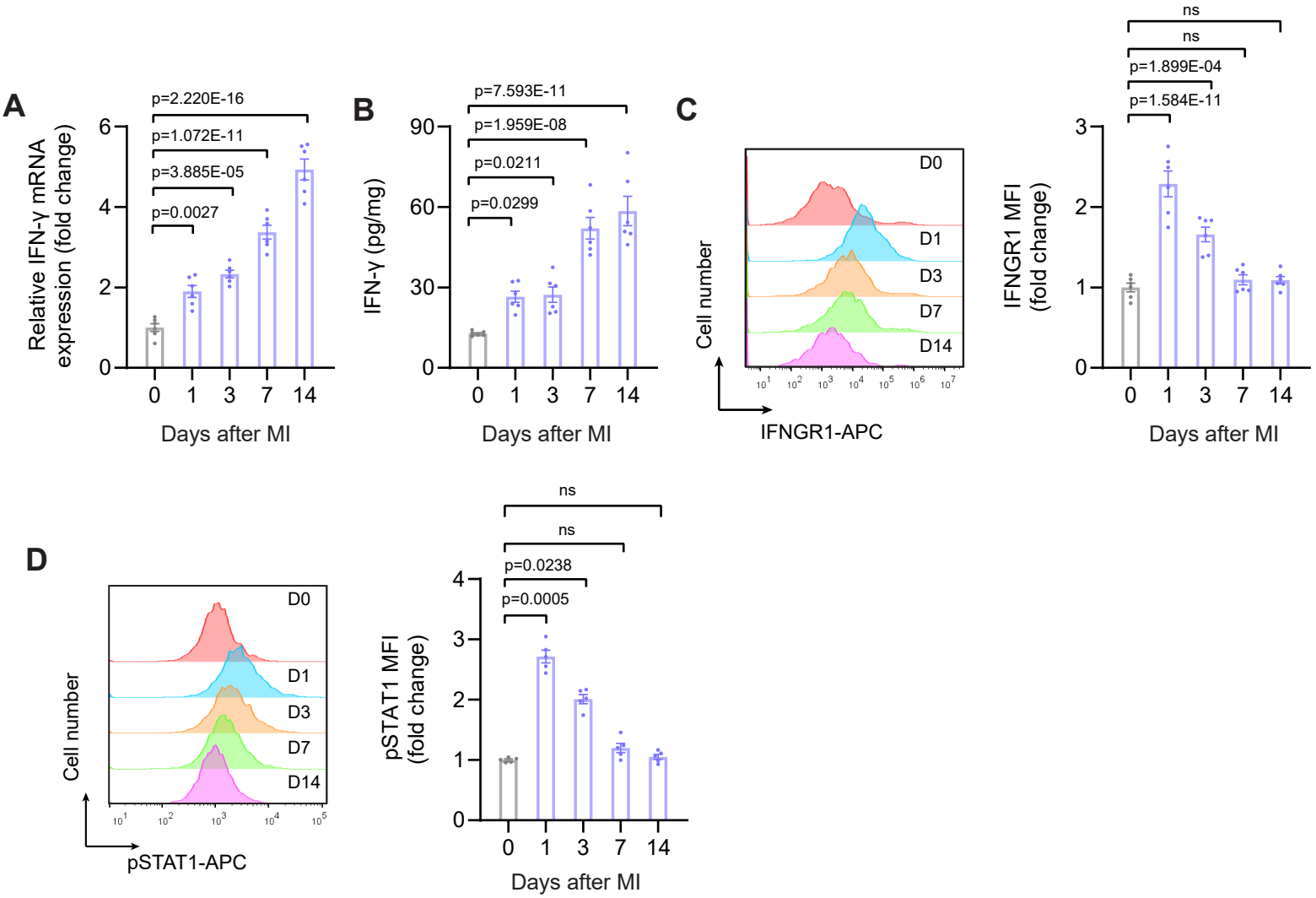
A
Relative IFN-γ mRNA expression (fold change)
p=2.220E-16
p=1.072E-11
p=3.885E-05
p=0.0027
Days after MI
B
IFN-γ (pg/mg)
p=7.593E-11
p=1.959E-08
p=0.0211
p=0.0299
Days after MI
C
Cell number
D0
D1
D3
D7
D14
IFNGR1-APC
IFNGR1 MFI (fold change)
ns
ns
p=1.899E-04
p=1.584E-11
Days after MI
D
Cell number
D0
D1
D3
D7
D14
pSTAT1-APC
pSTAT1 MFI (fold change)
ns
ns
p=0.0238
p=0.0005
Days after MI

Figure S14. Temporal dynamics of the type II interferon-STAT1 signaling pathway in cardiac macrophages after MI. A, Real-time PCR analysis of type II interferon (IFN-γ) expression in wild-type hearts before and after MI (n=6, each). **B,** ELISA analysis of IFN-γ expression in wild-type hearts pre- and post-MI (n=6, each). **C,** Time course changes of IFNGR1 expression in cardiac macrophages before and after MI (n=6, each). **D,** Time course changes of phosphorylated STAT1 in cardiac macrophages before and after MI (n=5, each). Data were analyzed using one-way ANOVA with Dunnett's multiple comparisons test (**A, B, C**) and Kruskal-Wallis test with Dunn's post hoc test (**D**).

Figure S15

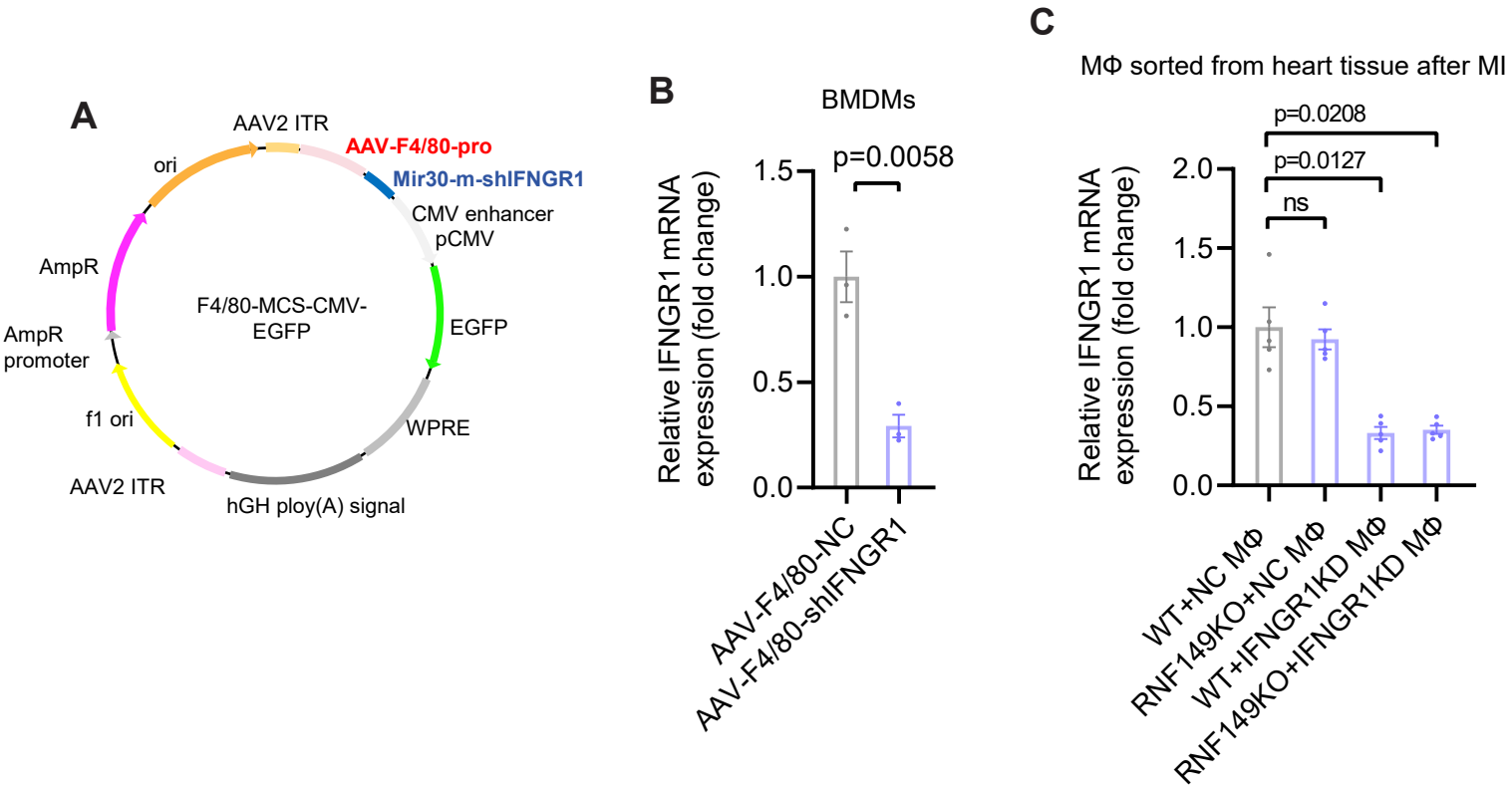
A
AAV2 ITR
AAV-F4/80-pro
Mir30-m-shIFNGR1
CMV enhancer
pCMV
EGFP
WPRE
hGH ploy(A) signal
AAV2 ITR
f1 ori
AmpR promoter
AmpR
ori
F4/80-MCS-CMV-EGFP
B
BMDMs
p=0.0058
Relative IFNGR1 mRNA expression (fold change)
1.5
1.0
0.5
0.0
AAV-F4/80-NC
AAV-F4/80-shIFNGR1
C
MΦ sorted from heart tissue after MI
p=0.0208
p=0.0127
ns
Relative IFNGR1 mRNA expression (fold change)
2.0
1.5
1.0
0.5
0.0
WT+NC MΦ
RNF149KO+NC MΦ
WT+IFNGR1KD MΦ
RNF149KO+IFNGR1KD MΦ

Figure S15. Efficacy of AAV encoding IFNGR1-shRNA driven by F4/80 promoter. A, Full sequence map for AAV-F4/80-miR30-m-shIFNGR1-eGFP (AAV-F4/80-shIFNGR1); The AAV system harbors a macrophage-specific F4/80 promoter, a miR30-based shRNA targeting IFNGR1, a cytomegalovirus promoter, and an enhanced GFP reporter. **B,** RT-PCR detected IFNGR1 mRNA expression in BMDMs from AAV-F4/80-shIFNGR1 or AAV-F4/80-NC-infected mice on day 28 after intra-BM injection. **C,** mRNA levels of IFNGR1 in infarct macrophages ($CD45^+CD11b^+Ly6G^-F4/80^+CD64^+$) from the designated groups according to the experimental setup in **Figure 7A**; n=5 per group. Data were analyzed using unpaired two-tailed student's t-test (**B**) and Kruskal-Wallis test with Dunn's post hoc test (**C**). BMDMs, bone marrow-derived macrophages; NC, negative control; KD, knockdown; ns, not significant.

Figure S16

A

> Mus musculus (mm10) RNF149 promoter region, strand (-) **STAT1-binding sites**

5'GCATGGGCCTGCAGAGACACCCCCTTCCCCCACACCTCACCACATACTCCCATAGAACATATCCCATCTTCTC
TTTATCTTTTTATAAACACATCATTGGAGGGACTGGGATTTAGAAACTCTGCAGGTTTGCATCCCACTCCAGCTAT
CACATGGAGATTCACACTCACTAGCCTAGAACTTGGAAGCCCCCGTTCCCCACTGGTCAGAGTAAACTTACATCT
GCATGCTCCCAACATACTGCTAGTTGAAGCTGGCACTCGAAGAGAGCAAGCAAGAAATCCTGGCCCTTATGAAG
GCCCCAAACCTTATTCCGAAATCAGTATTGGTAGCATGAAATTAATGTGCATACATATTATGCACAAGTGACATGG
GAAACCGAGCTTTTGTTAGCCCATGGTCAGCCAAGACAGGTTTTACAGAAGAAACAGCTGAAGGGTTAAAATTTC
AAAACCAATGTAGTGTTTGCCCGAACAAGAGGCAGAAGGAAGAGG**TCATTTCAGGAAGAA**GGAAATAATGTGTC — S7
AGACAGCAAGAAACCACAGC**GCTGTGTTCTGGGAACTAAAA**GCCTTTGCATTGCTGAAGCACAGCGCCAGGGG — S6
TTCTCGGGAGTGTTCCTCAGGCTGAAACACACCATCTTGTTCTGGGTCTAAAACATGGGAAAGGCCTTAACCTG
GAAATCCTATTGGCCTTTAAAACATGC**TTTCCTGGGGC**TGGGGCGATGGGTCAGTGGTTAAGAACCTAGGTTTG — S5
ATTCTGAGCACCCATATAGTGGCTGGCAATAGTCTATAACTCCAGTTCCAGGGCTAGTCAAGGGACATAAAACAT
ACATGGTGAATAGATATATATGCAGGCAAAACACTCACATACATAAAATAAAAATAAATACATTATTTTAGTAATGG
GAGTGGGAGAAGAGGTTTAACTTTAAAGCTACTCCTAGCTGGAACTCAGGCTGTGTCTCATACCACAGATGCAAT
CCAAAAGATAAAAAGAACCAGGTCTAACCTAAAACATATTGGTCTGGGCCCCAACAAAC**TACTTCCTGTAATTA**T — S4
AAACTCTTGCACAAAGAAGGAAGACTAGTGAGTCAATCAGAAATCAAAGCCCTGAACTTCATTTCCAGCTCCTTA
GTGGTTTGTTTGGTAGAAATAAAGAGACTGACGATGATTTCACGAATCACACAGTTTATTGCCACACAAAGGGGA
CTTTTGGCATTTGCTCACACTGAGTAAAGAGGGGGAAACAACATGAGCAAGCCTCACAGGGAACATGGTTCAGA
AATGCGGCAGCACAACGGCATAGTGAGTGAGTTTTGAAATCATGAGTTCAGTTGCTCCATCAGAATCGAAGCAG
GCCTCTGCTGAAAGTCCAGTGTAATTAAAGACTTGGTGTTCCTTTATAGAACTGGTTCTCAGGAGAAACTGGTTT
GACCAATACAACAGAGATCTGTGAGGTGACCTGAGGCCCCTCAGATAAAAAGGATAATATAAGTCAGGCTTAGG
GATGAGTTGAAGGTCTGTCACAGTATATGCCTGTGTGTGTATGTCTTCAGAATAGTGCCTAACAATGTATAGCTAT
GCATTAAGTCCATCACTTAAGTGTCCACTTCTTAGGTTTAAATACATTTTGATATTCAGTAGCTCATATATGAAGAG
GTATTTTAAATGTCTTTTGATATTTGGTAACTCGGGTGTGATGTCTCCTCAGCGTTATGGAGAGATCTCCTGTGTT
TATTCGGGTCTAGTCAGACTTCACATTC**TTCAAAGGAAA**TACCTTTCAGGTTCGCTGGGGTTGATCTACCAGAGC — S3
ATCTCAAATCTCAGCTCTACTCAAGAT**TTTACCGGAGC**AGAGTTACCATACTTGCATTTAACTATGTTTAGTGTGT — S2
TCAGGATCTTTTAATGGTACACTGAAAGTATCCACCCACTGTGTTGTCGAAGGACTATCTATCAGCCACCATTTAC
CTCCAAACAAATCCTTTCCCCTTTTTCCCCCCTTTTGATTAATGTAGCACCTTCGTCTTCGTCCAAACAGAGGCAC
ACATAAACTAAGGAGAAGGAAGAAAGGGCTCGAAGGCAACCATTGAGAAAAGAGCAACAAAGAATTTAATATATT
ACAGAGTTTGTAACAAAAGGCATCTGGACAACTTGACTTAGTGGTTTTTGTTGTTGTTTGCTTGTTTGTTTAAGTG
GTTTAGGCAGCCAGGCTTTTGCCGCGTGCCTTGCACAGTCAACTCCAC**CCTCTGAGAAA**CTTTACACAACCGCA — S1
GTCCCACGCTGGCCGACCCGGAGCGCACAAACTTCCCCAGACTTGGGGACTCTGGCAGCAGGGTTGCACAACT
CTCTGCAGCATCTGCAAGCTTCAGCTCGGCCGCCCACAGCCCTGCGGCACAGACCCTGGCGCCTGCGCACTCC
TCACGCCCGCGGGCAGGGCCCCACCCCTTCCGTCGCCACGCCCCGGTCACGCCCCTCCAGGTGCGCGTGCGC
CGCGGGTCCGCCCCCGCCGCGCTCGGCGGTCTCTCGCGAGCCGCCGCCGTCTCCTCAAAGCT3'

B

Primers used in ChIP-qPCR

P1: S1 primer-F: GAGTTGTGCAACCCTGCTG
S1 primer-R: TGCCTTGCACAGTCAACTC

P2: S2-3 primer-F: GTATGGTAACTCTGCTCCGGT
S2-3 primer-R: GTGTGATGTCTCCTCAGCGT

P3: S4 primer-F: CAGGGCTTTGATTTCTGATTGACT
S4 primer-R: TGTGTCTCATACCACAGATGCAA

P4: S5-7 primer-F: AACCACTGACCCATCGCC
S5-7 primer-R: AGGCAGAAGGAAGAGGTCAT

Figure S16. Analysis of STAT1-binding sites in *Rnf149* genomic loci. A, Identification of the putative STAT1-binding sites in the *Rnf149* promoter using the online TFBSs (transcription factor binding sites) analysis tool JASPAR. The *Rnf149* promoter region containing the STAT1-binding sites is displayed, with putative STAT1-binding sequences highlighted in red. **B,** ChIP-qPCR primers designed for amplification of *Rnf149* promoter fragments harboring the STAT1-binding sites.

Figure S17

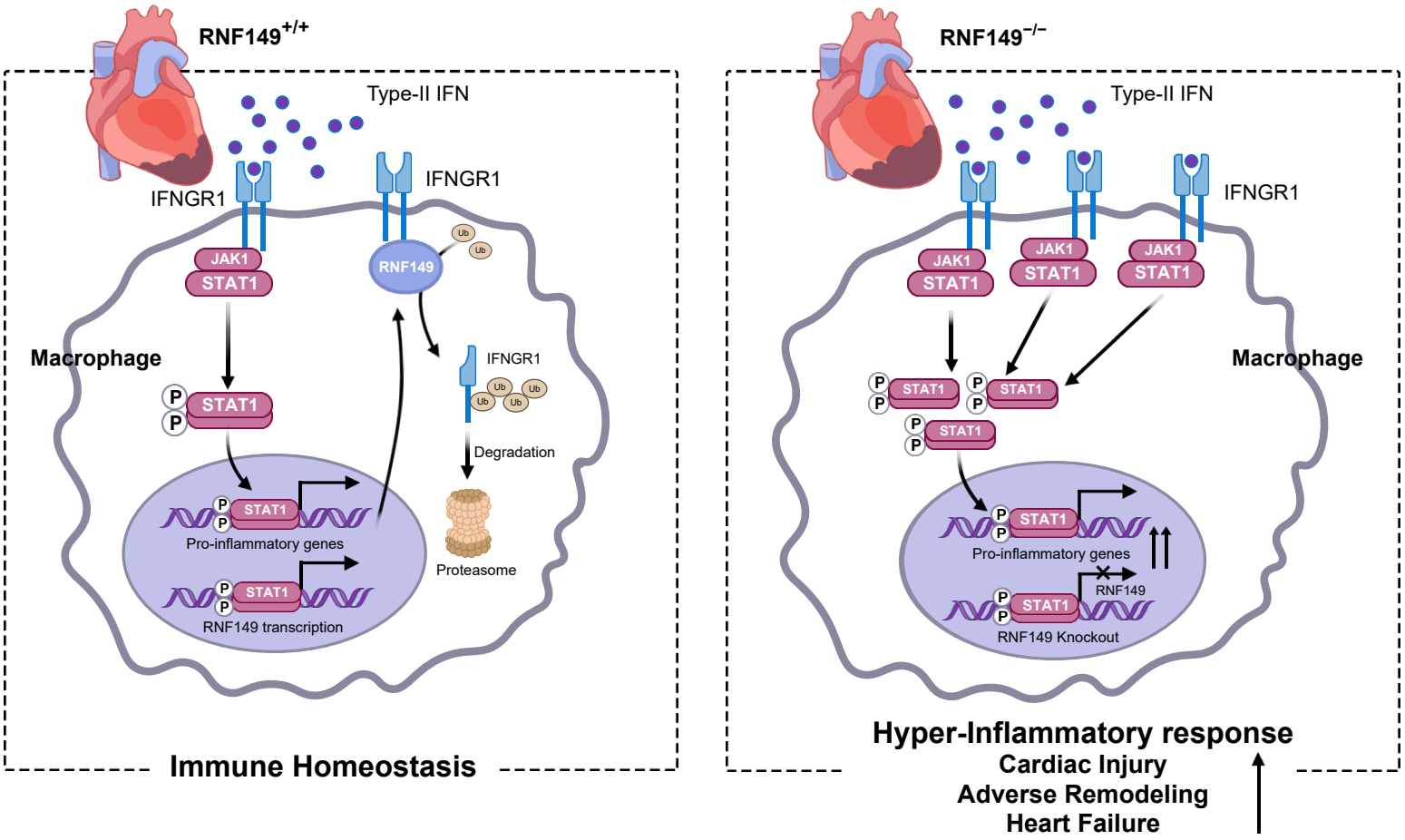
RNF149+/+
Type-II IFN
IFNGR1
IFNGR1
JAK1
STAT1
RNF149
Ub
Ub
Macrophage
P
P
STAT1
IFNGR1
Ub
Ub
Ub
Ub
Degradation
P
P
STAT1
Pro-inflammatory genes
Proteasome
P
P
STAT1
RNF149 transcription
Immune Homeostasis
RNF149−/−
Type-II IFN
IFNGR1
JAK1
STAT1
JAK1
STAT1
JAK1
STAT1
Macrophage
P
P
STAT1
P
P
STAT1
P
P
STAT1
P
P
STAT1
Pro-inflammatory genes
RNF149
P
P
STAT1
RNF149 Knockout
Hyper-Inflammatory response
Cardiac Injury
Adverse Remodeling
Heart Failure

Figure S17. Model of RNF149-mediated IFNGR1 destabilization in macrophage-driven inflammation following MI. The cartoon depicts the mechanisms by which RNF149 restrains macrophage inflammation and favors post-infarction cardiac repair. Acute MI stress activates the type-II IFN (IFN-γ) signaling pathway in cardiac macrophages, which triggers the pro-inflammatory activation of macrophages to mediate myocardial injury and remodeling after MI. In addition, STAT1 activation induces heightened expression of RNF149, which promotes the ubiquitination and proteasomal degradation of IFNGR1, acting as a negative feedback mechanism on type-II IFN signaling and macrophage-driven inflammation. Consequently, RNF149 loss-of-function augments the inflammatory response in macrophages, which exacerbates myocardial ischemic injury and impairs infarct healing, leading to maladaptive remodeling and heart failure.

List of Supplemental Tables

Table S1

Baseline echocardiographic parameters of RNF149KO and WT mice

Group	WT	RNF149KO
n	6	6
LVID;s (mm)	1.634±0.1046	1.657±0.0855
LVID;d (mm)	3.130±0.1044	3.184±0.0510
FS (%)	47.83±2.451	47.97±2.435
EDV (μl)	38.94±3.094	40.51±1.591
ESV (μl)	7.692±1.276	7.934±1.011
EF (%)	80.36±2.490	80.45±2.325
HR (bpm)	561±10	566±16

Results are presented as mean ± SEM.
LVID;s = left ventricular internal diameter at end-systole; ESV = end-systolic volume;
LVID;d = left ventricular internal diameter at end-diastole; EDV = end-diastolic volume;
FS = fractional shortening; EF = ejection fraction; HR = heart rate.

Table S2

Echocardiographic parameters of WT and RNF149KO mice after sham operation or 14 days post-MI

Group	WT sham	RNF149KO sham	WT MI	RNF149KO MI
n	6	6	8	8
LVID;s (mm)	1.610±0.0509	1.661±0.0482	3.965±0.1079	4.919±0.1294 p=1.461E-06 **
LVID;d (mm)	3.081±0.0581	3.161±0.0548	4.521±0.1174	5.301±0.1318 p=7.189E-05 **
FS (%)	47.73±1.306	47.47±1.158	12.53±0.7344	7.202±0.7621 p=0.0019 **
EDV (µl)	37.45±1.729	39.86±1.633	95.35±5.594	136.2±7.788 p=7.165E-05 **
ESV (µl)	7.360±0.6052	7.963±0.5791	70.49±4.172	114.7±7.095 p=1.827E-06 **
EF (%)	80.37±1.257	80.05±1.149	27.02±1.454	15.87±1.595 p=2.907E-05 **
HR (bpm)	577±8	579±14	580±12	575±14

Results are presented as mean ± SEM. Data were analyzed using two-way ANOVA with Bonferroni's multiple comparisons test.
** p versus WT MI.
LVID;s = left ventricular internal diameter at end-systole; LVID;d = left ventricular internal diameter at end-diastole;
FS = fractional shortening; EF = ejection fraction; EDV = end-diastolic volume; ESV = end-systolic volume; HR = heart rate.

Table S3

Echocardiographic parameters of mice with bone marrow transplantation 14 days post-MI

Group	WT-BM to WT	RNF149KO-BM to WT	WT-BM to RNF149KO	RNF149KO-BM to RNF149KO
n	8	8	8	8
LVID;s (mm)	3.842±0.1458	4.801±0.1602 p=0.0024 **	4.047±0.1654	4.984±0.1989 p=0.0031 ##
LVID;d (mm)	4.375±0.1550	5.201±0.1717 p=0.0173 *	4.623±0.1731	5.415±0.2109 p=0.0243 #
FS (%)	12.21±0.7047	7.680±0.7597 p=0.0006 **	12.49±0.7997	7.960±0.5305 p=0.0006 ##
EDV (μl)	87.66±7.357	131.0±9.913 p=0.0256 *	99.87±8.762	144.3±12.60 p=0.0208 #
ESV (μl)	64.58±6.006	108.8±8.231 p=0.0043 **	73.26±7.125	119.3±10.81 p=0.0029 ##
EF (%)	26.52±1.409	16.90±1.607 p=0.0004 **	26.94±1.604	17.47±1.119 p=0.0005 ##
HR (bpm)	574±10	562±16	572±18	581±13

Results are presented as mean ± SEM. Data were analyzed using two-way ANOVA with Bonferroni's multiple comparisons test.
*, ** p versus WT-BM to WT; #, ## p versus WT-BM to RNF149KO.
LVID;s = left ventricular internal diameter at end-systole; LVID;d = left ventricular internal diameter at end-diastole;
FS = fractional shortening; EF = ejection fraction; EDV = end-diastolic volume; ESV = end-systolic volume; HR = heart rate.

Table S4

Echocardiographic parameters of AAV-F4/80-NC and AAV-F4/80-shRNF149 mice after sham operation or 14 days post-MI

Group	AAV-F4/80-NC sham	AAV-F4/80-shRNF149 sham	AAV-F4/80-NC MI	AAV-F4/80-shRNF149 MI
n	6	6	7	7
LVID;s (mm)	1.588±0.0444	1.666±0.0354	3.745±0.1015	4.425±0.0924 p=1.366E-05 **
LVID;d (mm)	3.029±0.0412	3.125±0.0557	4.345±0.1149	4.893±0.1021 p=0.0010 **
FS (%)	47.61±0.8527	46.70±0.5659	13.83±0.7608	9.568±0.7424 p=0.0021 **
EDV (μl)	36.00±1.184	38.99±1.791	86.68±5.358	113.3±5.440 p=0.0008 **
ESV (μl)	7.243±0.5707	8.173±0.4178	60.99±3.755	89.59±4.182 p=4.185E-06 **
EF (%)	80.03±0.9965	79.03±0.5626	29.71±1.505	20.91±1.531 p=0.0003 **
HR (bpm)	588±7	572±11	580±9	579±15

Results are presented as mean ± SEM. Data were analyzed using two-way ANOVA with Bonferroni's multiple comparisons test.
** p versus AAV-F4/80-NC MI.
LVID;s = left ventricular internal diameter at end-systole; LVID;d = left ventricular internal diameter at end-diastole;
FS = fractional shortening; EF = ejection fraction; EDV = end-diastolic volume; ESV = end-systolic volume; HR = heart rate.

Table S5

Echocardiographic parameters of Adnull and AdRNF149 mice after sham operation or 14 days post-MI

Group	Adnull sham	AdRNF149 sham	Adnull MI	AdRNF149 MI
n	6	6	7	7
LVID;s (mm)	1.543±0.0407	1.598±0.0217	3.760±0.1029	3.191±0.0774 p=5.603E-05 **
LVID;d (mm)	2.849±0.0606	2.921±0.0315	4.248±0.0917	3.774±0.0665 p=0.0003 **
FS (%)	45.86±0.8305	45.30±0.3010	11.70±1.0193	15.85±0.7647 p=0.0059 **
EDV (µl)	31.00±1.612	32.86±0.8529	82.26±4.246	61.57±2.552 p=0.0001 **
ESV (µl)	6.592±0.4707	7.379±0.3068	62.06±3.710	41.24±2.261 p=1.041E-05 **
EF (%)	78.77±0.8651	77.58±0.4562	25.45±2.066	33.85±1.466 p=0.0019 **
HR (bpm)	573±21	567±16	571±18	569±14

Results are presented as mean ± SEM. Data were analyzed using two-way ANOVA with Bonferroni's multiple comparisons test.
** p versus Adnull MI.
LVID;s = left ventricular internal diameter at end-systole; LVID;d = left ventricular internal diameter at end-diastole;
FS = fractional shortening; EF = ejection fraction; EDV = end-diastolic volume; ESV = end-systolic volume; HR = heart rate.

Table S6

RNF149 protein interactome from BioGRID database

Interactor	Role	Organism	Experimental Evidence Code	Dataset	Throughput	HTP Score	Curated By
PRRG3	BAIT	H. sapiens	Affinity Capture-MS	Huttlin EL (2015)	High	0.768	BioGRID
TSPAN3	BAIT	H. sapiens	Affinity Capture-MS	Huttlin EL (2015)	High	0.991	BioGRID
TMEM231	BAIT	H. sapiens	Affinity Capture-MS	Huttlin EL (2015)	High	0.9759	BioGRID
TMEM30A	BAIT	H. sapiens	Affinity Capture-MS	Huttlin EL (2015)	High	0.9856	BioGRID
TSPAN17	BAIT	H. sapiens	Affinity Capture-MS	Huttlin EL (2015)	High	0.968	BioGRID
GINM1	BAIT	H. sapiens	Affinity Capture-MS	Huttlin EL (2015)	High	0.9644	BioGRID
BTNL8	BAIT	H. sapiens	Affinity Capture-MS	Huttlin EL (2015)	High	0.9992	BioGRID
TNFRSF10B	BAIT	H. sapiens	Affinity Capture-MS	Huttlin EL (2015)	High	0.9984	BioGRID
HEPACAM2	BAIT	H. sapiens	Affinity Capture-MS	Huttlin EL (2015)	High	0.9878	BioGRID
ACVR1	BAIT	H. sapiens	Affinity Capture-MS	Huttlin EL (2015)	High	0.9913	BioGRID
BTNL8	BAIT	H. sapiens	Affinity Capture-MS	Huttlin EL (2017)	High	0.9961	BioGRID
MANSC1	BAIT	H. sapiens	Affinity Capture-MS	Huttlin EL (2017)	High	0.9961	BioGRID
TNFRSF10B	BAIT	H. sapiens	Affinity Capture-MS	Huttlin EL (2017)	High	0.9953	BioGRID
PCDHGB4	BAIT	H. sapiens	Affinity Capture-MS	Huttlin EL (2017)	High	0.9869	BioGRID
TNFRSF10A	BAIT	H. sapiens	Affinity Capture-MS	Huttlin EL (2017)	High	0.9534	BioGRID
MRAP2	BAIT	H. sapiens	Affinity Capture-MS	Huttlin EL (2017)	High	0.9453	BioGRID
HLA-DRB1	BAIT	H. sapiens	Affinity Capture-MS	Huttlin EL (2017)	High	0.944	BioGRID
TSPAN3	BAIT	H. sapiens	Affinity Capture-MS	Huttlin EL (2017)	High	0.9376	BioGRID
ACVR1	BAIT	H. sapiens	Affinity Capture-MS	Huttlin EL (2017)	High	0.9376	BioGRID
ARRDC3	BAIT	H. sapiens	Affinity Capture-MS	Huttlin EL (2017)	High	0.9373	BioGRID
PCDHB7	BAIT	H. sapiens	Affinity Capture-MS	Huttlin EL (2017)	High	0.9278	BioGRID
TMEM30A	BAIT	H. sapiens	Affinity Capture-MS	Huttlin EL (2017)	High	0.9123	BioGRID
HEPACAM2	BAIT	H. sapiens	Affinity Capture-MS	Huttlin EL (2017)	High	0.9057	BioGRID
TPCN2	BAIT	H. sapiens	Affinity Capture-MS	Huttlin EL (2017)	High	0.9005	BioGRID
LITAF	BAIT	H. sapiens	Affinity Capture-MS	Huttlin EL (2017)	High	0.8926	BioGRID
TMEM231	BAIT	H. sapiens	Affinity Capture-MS	Huttlin EL (2017)	High	0.8879	BioGRID
IL17RB	BAIT	H. sapiens	Affinity Capture-MS	Huttlin EL (2017)	High	0.884	BioGRID
SLC20A1	BAIT	H. sapiens	Affinity Capture-MS	Huttlin EL (2017)	High	0.8825	BioGRID
C16ORF58	BAIT	H. sapiens	Affinity Capture-MS	Huttlin EL (2017)	High	0.8672	BioGRID
LMAN2L	BAIT	H. sapiens	Affinity Capture-MS	Huttlin EL (2017)	High	0.8617	BioGRID
GINM1	BAIT	H. sapiens	Affinity Capture-MS	Huttlin EL (2017)	High	0.8157	BioGRID
TSPAN17	BAIT	H. sapiens	Affinity Capture-MS	Huttlin EL (2017)	High	0.8021	BioGRID
RNF4	BAIT	H. sapiens	Affinity Capture-MS	Kumar R (2017)	High	-	BioGRID
LAMP1	BAIT	H. sapiens	Affinity Capture-MS	Liu X (2018)	High	-	BioGRID
ADCY6	HIT	H. sapiens	Affinity Capture-MS	Huttlin EL (2021)	High	0.9988	BioGRID
ADCY9	HIT	H. sapiens	Affinity Capture-MS	Huttlin EL (2021)	High	0.862	BioGRID
TMEM30A	BAIT	H. sapiens	Affinity Capture-MS	Huttlin EL (2021)	High	0.8199	BioGRID
TGFBR2	HIT	H. sapiens	Affinity Capture-MS	Huttlin EL (2021)	High	1	BioGRID
ANKRD46	HIT	H. sapiens	Affinity Capture-MS	Huttlin EL (2021)	High	0.8968	BioGRID
TSPAN3	BAIT	H. sapiens	Affinity Capture-MS	Huttlin EL (2021)	High	0.8258	BioGRID
TFB2M	HIT	H. sapiens	Affinity Capture-MS	Huttlin EL (2021)	High	0.9466	BioGRID
CCDC85C	HIT	H. sapiens	Affinity Capture-MS	Huttlin EL (2021)	High	0.9781	BioGRID
PTPRA	HIT	H. sapiens	Affinity Capture-MS	Huttlin EL (2021)	High	0.9901	BioGRID
TUBGCP3	HIT	H. sapiens	Affinity Capture-MS	Huttlin EL (2021)	High	0.8128	BioGRID
TNFRSF10B	BAIT	H. sapiens	Affinity Capture-MS	Huttlin EL (2021)	High	0.999	BioGRID
NR2F2	HIT	H. sapiens	Affinity Capture-MS	Huttlin EL (2021)	High	0.982	BioGRID
RBM25	HIT	H. sapiens	Affinity Capture-MS	Huttlin EL (2021)	High	0.9979	BioGRID
ZDHHC13	HIT	H. sapiens	Affinity Capture-MS	Huttlin EL (2021)	High	0.9424	BioGRID
CCDC91	HIT	H. sapiens	Affinity Capture-MS	Huttlin EL (2021)	High	1	BioGRID
BMPR1A	HIT	H. sapiens	Affinity Capture-MS	Huttlin EL (2021)	High	0.999	BioGRID
BNIP3L	HIT	H. sapiens	Affinity Capture-MS	Huttlin EL (2021)	High	0.9998	BioGRID
BNIP3	HIT	H. sapiens	Affinity Capture-MS	Huttlin EL (2021)	High	0.9172	BioGRID
LITAF	BAIT	H. sapiens	Affinity Capture-MS	Huttlin EL (2021)	High	0.799	BioGRID
MRAP2	BAIT	H. sapiens	Affinity Capture-MS	Huttlin EL (2021)	High	0.8463	BioGRID
BROX	HIT	H. sapiens	Affinity Capture-MS	Huttlin EL (2021)	High	0.8203	BioGRID
PLXNB2	HIT	H. sapiens	Affinity Capture-MS	Huttlin EL (2021)	High	0.9497	BioGRID
CRLF2	BAIT	H. sapiens	Affinity Capture-MS	Huttlin EL (2021)	High	0.9696	BioGRID
PPP1R13B	HIT	H. sapiens	Affinity Capture-MS	Huttlin EL (2021)	High	0.9999	BioGRID
CTLA4	BAIT	H. sapiens	Affinity Capture-MS	Huttlin EL (2021)	High	0.8549	BioGRID
NAMPT	HIT	H. sapiens	Affinity Capture-MS	Huttlin EL (2021)	High	0.9101	BioGRID
RELT	HIT	H. sapiens	Affinity Capture-MS	Huttlin EL (2021)	High	0.9158	BioGRID
TUBB1	HIT	H. sapiens	Affinity Capture-MS	Huttlin EL (2021)	High	1	BioGRID
ARL17A	HIT	H. sapiens	Affinity Capture-MS	Huttlin EL (2021)	High	0.9986	BioGRID
PVRL3	HIT	H. sapiens	Affinity Capture-MS	Huttlin EL (2021)	High	0.9913	BioGRID
JAK1	HIT	H. sapiens	Affinity Capture-MS	Huttlin EL (2021)	High	0.9984	BioGRID
LRP10	HIT	H. sapiens	Affinity Capture-MS	Huttlin EL (2021)	High	0.9882	BioGRID
ABCA3	HIT	H. sapiens	Affinity Capture-MS	Huttlin EL (2021)	High	0.9318	BioGRID
USP8	HIT	H. sapiens	Affinity Capture-MS	Huttlin EL (2021)	High	0.9998	BioGRID
VAMP3	HIT	H. sapiens	Affinity Capture-MS	Huttlin EL (2021)	High	0.8907	BioGRID
RAB2A	HIT	H. sapiens	Affinity Capture-MS	Huttlin EL (2021)	High	0.9927	BioGRID
SMIM5	BAIT	H. sapiens	Affinity Capture-MS	Huttlin EL (2021)	High	0.8628	BioGRID
EPHB4	HIT	H. sapiens	Affinity Capture-MS	Huttlin EL (2021)	High	0.9936	BioGRID
ZDHHC9	BAIT	H. sapiens	Affinity Capture-MS	Huttlin EL (2021/pre-pub)	High	0.7575	BioGRID
ACKR3	BAIT	H. sapiens	Affinity Capture-MS	Huttlin EL (2021/pre-pub)	High	0.9923	BioGRID
CLDN14	BAIT	H. sapiens	Affinity Capture-MS	Huttlin EL (2021/pre-pub)	High	0.9883	BioGRID
CDRT15	BAIT	H. sapiens	Affinity Capture-MS	Huttlin EL (2021/pre-pub)	High	0.8598	BioGRID
CTLA4	BAIT	H. sapiens	Affinity Capture-MS	Huttlin EL (2021/pre-pub)	High	0.599	BioGRID
TBXA2R	BAIT	H. sapiens	Affinity Capture-MS	Huttlin EL (2021/pre-pub)	High	0.6328	BioGRID
LRRC52	BAIT	H. sapiens	Affinity Capture-MS	Huttlin EL (2021/pre-pub)	High	0.6088	BioGRID
HFE	BAIT	H. sapiens	Affinity Capture-MS	Huttlin EL (2021/pre-pub)	High	0.9871	BioGRID
ICAM3	BAIT	H. sapiens	Affinity Capture-MS	Huttlin EL (2021/pre-pub)	High	0.553	BioGRID
C16ORF58	BAIT	H. sapiens	Affinity Capture-MS	Huttlin EL (2021/pre-pub)	High	0.9111	BioGRID
PDGFRB	BAIT	H. sapiens	Affinity Capture-MS	Huttlin EL (2021/pre-pub)	High	0.9724	BioGRID
KIAA0391	BAIT	H. sapiens	Affinity Capture-MS	Huttlin EL (2021/pre-pub)	High	0.9827	BioGRID
FLOT1	HIT	H. sapiens	Affinity Capture-MS	Huttlin EL (2021/pre-pub)	High	0.6071	BioGRID
ATP2B4	HIT	H. sapiens	Affinity Capture-MS	Huttlin EL (2021/pre-pub)	High	0.9808	BioGRID
ATP2B2	HIT	H. sapiens	Affinity Capture-MS	Huttlin EL (2021/pre-pub)	High	0.9939	BioGRID
NDFIP1	HIT	H. sapiens	Affinity Capture-MS	Huttlin EL (2021/pre-pub)	High	1	BioGRID
PTPRA	HIT	H. sapiens	Affinity Capture-MS	Huttlin EL (2021/pre-pub)	High	0.9947	BioGRID
YES1	HIT	H. sapiens	Affinity Capture-MS	Huttlin EL (2021/pre-pub)	High	0.9597	BioGRID
FGFR2	HIT	H. sapiens	Affinity Capture-MS	Huttlin EL (2021/pre-pub)	High	1	BioGRID
FGFR4	HIT	H. sapiens	Affinity Capture-MS	Huttlin EL (2021/pre-pub)	High	0.8792	BioGRID
SLC12A2	HIT	H. sapiens	Affinity Capture-MS	Huttlin EL (2021/pre-pub)	High	0.6138	BioGRID
JAK1	HIT	H. sapiens	Affinity Capture-MS	Huttlin EL (2021/pre-pub)	High	0.9989	BioGRID
PLXNB2	HIT	H. sapiens	Affinity Capture-MS	Huttlin EL (2021/pre-pub)	High	0.5469	BioGRID
SLC39A4	HIT	H. sapiens	Affinity Capture-MS	Huttlin EL (2021/pre-pub)	High	0.9066	BioGRID
OSMR	HIT	H. sapiens	Affinity Capture-MS	Huttlin EL (2021/pre-pub)	High	0.9552	BioGRID
PTPRS	HIT	H. sapiens	Affinity Capture-MS	Huttlin EL (2021/pre-pub)	High	1	BioGRID
PTPRF	HIT	H. sapiens	Affinity Capture-MS	Huttlin EL (2021/pre-pub)	High	0.9973	BioGRID
PTPRG	HIT	H. sapiens	Affinity Capture-MS	Huttlin EL (2021/pre-pub)	High	0.9995	BioGRID
SLC12A7	HIT	H. sapiens	Affinity Capture-MS	Huttlin EL (2021/pre-pub)	High	0.9713	BioGRID
DDR1	HIT	H. sapiens	Affinity Capture-MS	Huttlin EL (2021/pre-pub)	High	0.9978	BioGRID
USP8	HIT	H. sapiens	Affinity Capture-MS	Huttlin EL (2021/pre-pub)	High	0.9985	BioGRID
MYRF	HIT	H. sapiens	Affinity Capture-MS	Huttlin EL (2021/pre-pub)	High	1	BioGRID
CSNK1G3	HIT	H. sapiens	Affinity Capture-MS	Huttlin EL (2021/pre-pub)	High	1	BioGRID
ANKRD13A	HIT	H. sapiens	Affinity Capture-MS	Huttlin EL (2021/pre-pub)	High	0.87	BioGRID
EPHB4	HIT	H. sapiens	Affinity Capture-MS	Huttlin EL (2021/pre-pub)	High	0.9837	BioGRID
TNFRSF10B	HIT	H. sapiens	Affinity Capture-MS	Huttlin EL (2021/pre-pub)	High	0.9924	BioGRID
BMPR1A	HIT	H. sapiens	Affinity Capture-MS	Huttlin EL (2021/pre-pub)	High	0.9999	BioGRID
TNFRSF21	HIT	H. sapiens	Affinity Capture-MS	Huttlin EL (2021/pre-pub)	High	0.954	BioGRID
PTPRE	HIT	H. sapiens	Affinity Capture-MS	Huttlin EL (2021/pre-pub)	High	0.9863	BioGRID
NOTCH2	HIT	H. sapiens	Affinity Capture-MS	Huttlin EL (2021/pre-pub)	High	0.6803	BioGRID
SLC20A1	HIT	H. sapiens	Affinity Capture-MS	Huttlin EL (2021/pre-pub)	High	0.934	BioGRID
GNA13	HIT	H. sapiens	Affinity Capture-MS	Huttlin EL (2021/pre-pub)	High	0.4113	BioGRID
UGCG	HIT	H. sapiens	Affinity Capture-MS	Huttlin EL (2021/pre-pub)	High	0.9988	BioGRID
RAB2A	HIT	H. sapiens	Affinity Capture-MS	Huttlin EL (2021/pre-pub)	High	0.4107	BioGRID
ELFN2	HIT	H. sapiens	Affinity Capture-MS	Huttlin EL (2021/pre-pub)	High	0.9959	BioGRID
ACVR1B	HIT	H. sapiens	Affinity Capture-MS	Huttlin EL (2021/pre-pub)	High	0.9905	BioGRID
SNX27	HIT	H. sapiens	Affinity Capture-MS	Huttlin EL (2021/pre-pub)	High	0.9995	BioGRID
KIDINS220	HIT	H. sapiens	Affinity Capture-MS	Huttlin EL (2021/pre-pub)	High	0.9941	BioGRID
TMEM200A	HIT	H. sapiens	Affinity Capture-MS	Huttlin EL (2021/pre-pub)	High	0.9998	BioGRID
IFNGR1	HIT	H. sapiens	Affinity Capture-MS	Huttlin EL (2021/pre-pub)	High	0.9891	BioGRID
VAMP7	HIT	H. sapiens	Affinity Capture-MS	Huttlin EL (2021/pre-pub)	High	0.9517	BioGRID
UNC5B	HIT	H. sapiens	Affinity Capture-MS	Huttlin EL (2021/pre-pub)	High	0.9999	BioGRID
LRP10	HIT	H. sapiens	Affinity Capture-MS	Huttlin EL (2021/pre-pub)	High	1	BioGRID
ACVR1	HIT	H. sapiens	Affinity Capture-MS	Huttlin EL (2021/pre-pub)	High	0.9921	BioGRID
CACNG6	BAIT	H. sapiens	Affinity Capture-MS	Huttlin EL (2021/pre-pub)	High	0.9999	BioGRID
IL3RA	BAIT	H. sapiens	Affinity Capture-MS	Huttlin EL (2021/pre-pub)	High	0.8929	BioGRID
CD8A	BAIT	H. sapiens	Affinity Capture-MS	Huttlin EL (2021/pre-pub)	High	0.8247	BioGRID
CABP2	BAIT	H. sapiens	Affinity Capture-MS	Huttlin EL (2021/pre-pub)	High	0.8991	BioGRID
GJA8	BAIT	H. sapiens	Affinity Capture-MS	Huttlin EL (2021/pre-pub)	High	0.9885	BioGRID
RGS9BP	BAIT	H. sapiens	Affinity Capture-MS	Huttlin EL (2021/pre-pub)	High	0.981	BioGRID
IL17RD	BAIT	H. sapiens	Affinity Capture-MS	Huttlin EL (2021/pre-pub)	High	0.843	BioGRID
IL4R	BAIT	H. sapiens	Affinity Capture-MS	Huttlin EL (2021/pre-pub)	High	0.9003	BioGRID
TMEM52B	BAIT	H. sapiens	Affinity Capture-MS	Huttlin EL (2021/pre-pub)	High	0.9143	BioGRID
MUC1	BAIT	H. sapiens	Affinity Capture-MS	Huttlin EL (2021/pre-pub)	High	0.8388	BioGRID
TMEM30B	BAIT	H. sapiens	Affinity Capture-MS	Huttlin EL (2021/pre-pub)	High	0.91	BioGRID
PTGFR	BAIT	H. sapiens	Affinity Capture-MS	Huttlin EL (2021/pre-pub)	High	0.9142	BioGRID
OPN4	BAIT	H. sapiens	Affinity Capture-MS	Huttlin EL (2021/pre-pub)	High	0.9854	BioGRID
NOX4	BAIT	H. sapiens	Affinity Capture-MS	Huttlin EL (2021/pre-pub)	High	0.9035	BioGRID
MEGF9	BAIT	H. sapiens	Affinity Capture-MS	Huttlin EL (2021/pre-pub)	High	0.6192	BioGRID
NMUR1	BAIT	H. sapiens	Affinity Capture-MS	Huttlin EL (2021/pre-pub)	High	0.9081	BioGRID
NKAIN1	BAIT	H. sapiens	Affinity Capture-MS	Huttlin EL (2021/pre-pub)	High	0.9878	BioGRID
TMEM192	BAIT	H. sapiens	Affinity Capture-MS	Zellner S (2021)	High	-	BioGRID
CANX	BAIT	H. sapiens	Affinity Capture-MS	Cho NH (2022)	High	-	BioGRID

RNF149 protein interactome from BioGRID database

PTPRS	HIT	H. sapiens	Affinity Capture-MS	Huttlin EL (2021)	High	0.9983	BioGRID
PRPF40A	HIT	H. sapiens	Affinity Capture-MS	Huttlin EL (2021)	High	0.9652	BioGRID
RNF128	HIT	H. sapiens	Affinity Capture-MS	Huttlin EL (2021)	High	0.9986	BioGRID
LSMEM2	BAIT	H. sapiens	Affinity Capture-MS	Huttlin EL (2021)	High	0.9998	BioGRID
UNC5B	HIT	H. sapiens	Affinity Capture-MS	Huttlin EL (2021)	High	0.9999	BioGRID
DUOXA2	BAIT	H. sapiens	Affinity Capture-MS	Huttlin EL (2021)	High	0.8381	BioGRID
ARRDC3	BAIT	H. sapiens	Affinity Capture-MS	Huttlin EL (2021)	High	0.815	BioGRID
LGR4	HIT	H. sapiens	Affinity Capture-MS	Huttlin EL (2021)	High	0.8843	BioGRID
NDFIP1	HIT	H. sapiens	Affinity Capture-MS	Huttlin EL (2021)	High	0.9899	BioGRID
FGFR2	HIT	H. sapiens	Affinity Capture-MS	Huttlin EL (2021)	High	0.9312	BioGRID
TOM1	BAIT	H. sapiens	Affinity Capture-MS	Huttlin EL (2021)	High	0.831	BioGRID
NBR1	HIT	H. sapiens	Affinity Capture-MS	Huttlin EL (2021)	High	0.9946	BioGRID
LMAN2L	BAIT	H. sapiens	Affinity Capture-MS	Huttlin EL (2021)	High	0.9779	BioGRID
NRSN2	HIT	H. sapiens	Affinity Capture-MS	Huttlin EL (2021)	High	0.9469	BioGRID
RNF19A	HIT	H. sapiens	Affinity Capture-MS	Huttlin EL (2021)	High	0.9999	BioGRID
STXBP3	HIT	H. sapiens	Affinity Capture-MS	Huttlin EL (2021)	High	0.7884	BioGRID
SNX3	HIT	H. sapiens	Affinity Capture-MS	Huttlin EL (2021)	High	0.9934	BioGRID
ABCD4	BAIT	H. sapiens	Affinity Capture-MS	Huttlin EL (2021)	High	1	BioGRID
RGS9BP	BAIT	H. sapiens	Affinity Capture-MS	Huttlin EL (2021)	High	0.9812	BioGRID
PCDHGB4	BAIT	H. sapiens	Affinity Capture-MS	Huttlin EL (2021)	High	0.9378	BioGRID
RNF133	BAIT	H. sapiens	Affinity Capture-MS	Huttlin EL (2021)	High	0.8684	BioGRID
PIGN	HIT	H. sapiens	Affinity Capture-MS	Huttlin EL (2021)	High	0.9822	BioGRID
GOSR1	HIT	H. sapiens	Affinity Capture-MS	Huttlin EL (2021)	High	0.891	BioGRID
HLA-DRB1	BAIT	H. sapiens	Affinity Capture-MS	Huttlin EL (2021)	High	0.8205	BioGRID
STX12	HIT	H. sapiens	Affinity Capture-MS	Huttlin EL (2021)	High	0.7577	BioGRID
TTYH1	BAIT	H. sapiens	Affinity Capture-MS	Huttlin EL (2021)	High	0.9511	BioGRID
CC2D1A	HIT	H. sapiens	Affinity Capture-MS	Huttlin EL (2021)	High	1	BioGRID
PTPRF	HIT	H. sapiens	Affinity Capture-MS	Huttlin EL (2021)	High	0.9978	BioGRID
BMPR2	HIT	H. sapiens	Affinity Capture-MS	Huttlin EL (2021)	High	0.9999	BioGRID
TMEM74	BAIT	H. sapiens	Affinity Capture-MS	Huttlin EL (2021)	High	0.9965	BioGRID
ACVR2B	HIT	H. sapiens	Affinity Capture-MS	Huttlin EL (2021)	High	0.968	BioGRID
ACVR2A	HIT	H. sapiens	Affinity Capture-MS	Huttlin EL (2021)	High	0.9933	BioGRID
ACVR1B	HIT	H. sapiens	Affinity Capture-MS	Huttlin EL (2021)	High	0.8255	BioGRID
FGFR1	HIT	H. sapiens	Affinity Capture-MS	Huttlin EL (2021)	High	0.7808	BioGRID
PLXNA4	HIT	H. sapiens	Affinity Capture-MS	Huttlin EL (2021)	High	0.9995	BioGRID
SLC12A2	HIT	H. sapiens	Affinity Capture-MS	Huttlin EL (2021)	High	0.7766	BioGRID
GOLGA5	HIT	H. sapiens	Affinity Capture-MS	Huttlin EL (2021)	High	0.9719	BioGRID
CDC6	HIT	H. sapiens	Affinity Capture-MS	Huttlin EL (2021)	High	0.9058	BioGRID
AKIRIN2	HIT	H. sapiens	Affinity Capture-MS	Huttlin EL (2021)	High	1	BioGRID
NDFIP2	HIT	H. sapiens	Affinity Capture-MS	Huttlin EL (2021)	High	0.8758	BioGRID
LSR	HIT	H. sapiens	Affinity Capture-MS	Huttlin EL (2021)	High	0.8411	BioGRID
STX6	HIT	H. sapiens	Affinity Capture-MS	Huttlin EL (2021)	High	0.9865	BioGRID
ADIPOR1	HIT	H. sapiens	Affinity Capture-MS	Huttlin EL (2021)	High	0.99	BioGRID
TMEM183A	HIT	H. sapiens	Affinity Capture-MS	Huttlin EL (2021)	High	1	BioGRID
CERK	HIT	H. sapiens	Affinity Capture-MS	Huttlin EL (2021)	High	0.9992	BioGRID
NARS2	HIT	H. sapiens	Affinity Capture-MS	Huttlin EL (2021)	High	0.9986	BioGRID
UPK3BL	HIT	H. sapiens	Affinity Capture-MS	Huttlin EL (2021)	High	0.93	BioGRID
SLC20A1	BAIT	H. sapiens	Affinity Capture-MS	Huttlin EL (2021)	High	0.8365	BioGRID
NOMO1	HIT	H. sapiens	Affinity Capture-MS	Huttlin EL (2021)	High	0.8268	BioGRID
HEPACAM2	BAIT	H. sapiens	Affinity Capture-MS	Huttlin EL (2021)	High	0.8142	BioGRID
GRK6	HIT	H. sapiens	Affinity Capture-MS	Huttlin EL (2021)	High	0.9978	BioGRID
SLC20A2	HIT	H. sapiens	Affinity Capture-MS	Huttlin EL (2021)	High	0.9513	BioGRID
ATP2B4	HIT	H. sapiens	Affinity Capture-MS	Huttlin EL (2021)	High	0.8974	BioGRID
CSNK1E	HIT	H. sapiens	Affinity Capture-MS	Huttlin EL (2021)	High	0.8166	BioGRID
HSDL1	HIT	H. sapiens	Affinity Capture-MS	Huttlin EL (2021)	High	0.9199	BioGRID
ACVR1	BAIT	H. sapiens	Affinity Capture-MS	Huttlin EL (2021)	High	0.9999	BioGRID
COX1	HIT	H. sapiens	Affinity Capture-MS	Huttlin EL (2021)	High	0.8049	BioGRID
HFE	BAIT	H. sapiens	Affinity Capture-MS	Huttlin EL (2021)	High	0.9775	BioGRID
STARD3	HIT	H. sapiens	Affinity Capture-MS	Huttlin EL (2021)	High	0.943	BioGRID
CSNK1G1	HIT	H. sapiens	Affinity Capture-MS	Huttlin EL (2021)	High	0.9997	BioGRID
TBC1D22B	HIT	H. sapiens	Affinity Capture-MS	Huttlin EL (2021)	High	1	BioGRID
FYN	HIT	H. sapiens	Affinity Capture-MS	Huttlin EL (2021)	High	0.9635	BioGRID
RNF19B	HIT	H. sapiens	Affinity Capture-MS	Huttlin EL (2021)	High	0.9975	BioGRID
DGAT1	HIT	H. sapiens	Affinity Capture-MS	Huttlin EL (2021)	High	0.9996	BioGRID
RAB2B	HIT	H. sapiens	Affinity Capture-MS	Huttlin EL (2021)	High	1	BioGRID
ATP12A	HIT	H. sapiens	Affinity Capture-MS	Huttlin EL (2021)	High	0.8594	BioGRID
MFAP3	HIT	H. sapiens	Affinity Capture-MS	Huttlin EL (2021)	High	0.9669	BioGRID
MARCH1	BAIT	H. sapiens	Affinity Capture-MS	Huttlin EL (2021)	High	0.9924	BioGRID
EDAR	BAIT	H. sapiens	Affinity Capture-MS	Huttlin EL (2021)	High	0.8606	BioGRID
NRSN1	BAIT	H. sapiens	Affinity Capture-MS	Huttlin EL (2021)	High	0.9982	BioGRID
HUS1	HIT	H. sapiens	Affinity Capture-MS	Huttlin EL (2021)	High	0.9976	BioGRID
MANSC1	BAIT	H. sapiens	Affinity Capture-MS	Huttlin EL (2021)	High	0.972	BioGRID
NOTCH2	HIT	H. sapiens	Affinity Capture-MS	Huttlin EL (2021)	High	0.9857	BioGRID

BTNL8	BAIT	H. sapiens	Affinity Capture-MS	Huttlin EL (2021)	High	0.9858	BioGRID
IFNGR1	BAIT	H. sapiens	Affinity Capture-MS	Huttlin EL (2021)	High	0.9791	BioGRID
SDCBP	HIT	H. sapiens	Affinity Capture-MS	Huttlin EL (2021)	High	0.9156	BioGRID
ZDHHC12	BAIT	H. sapiens	Affinity Capture-MS	Huttlin EL (2021)	High	0.877	BioGRID
PCDHA8	BAIT	H. sapiens	Affinity Capture-MS	Huttlin EL (2021)	High	0.9288	BioGRID
RET	BAIT	H. sapiens	Affinity Capture-MS	Huttlin EL (2021)	High	0.9389	BioGRID
DLK1	BAIT	H. sapiens	Affinity Capture-MS	Huttlin EL (2021)	High	0.9988	BioGRID
HLA-C	BAIT	H. sapiens	Affinity Capture-MS	Huttlin EL (2021)	High	0.9919	BioGRID
CSNK1G2	BAIT	H. sapiens	Affinity Capture-MS	Huttlin EL (2021)	High	0.9997	BioGRID
SGCA	BAIT	H. sapiens	Affinity Capture-MS	Huttlin EL (2021)	High	0.9445	BioGRID
HLA-DPB1	BAIT	H. sapiens	Affinity Capture-MS	Huttlin EL (2021)	High	0.9997	BioGRID
GPM6A	BAIT	H. sapiens	Affinity Capture-MS	Huttlin EL (2021)	High	0.9578	BioGRID
CD3E	BAIT	H. sapiens	Affinity Capture-MS	Huttlin EL (2021)	High	0.9987	BioGRID
CLDND1	BAIT	H. sapiens	Affinity Capture-MS	Huttlin EL (2021)	High	0.971	BioGRID
SFTPC	BAIT	H. sapiens	Affinity Capture-MS	Huttlin EL (2021)	High	0.9686	BioGRID
HLA-DRB3	BAIT	H. sapiens	Affinity Capture-MS	Huttlin EL (2021)	High	0.9857	BioGRID
KCNE3	BAIT	H. sapiens	Affinity Capture-MS	Huttlin EL (2021)	High	0.9996	BioGRID
TMPRSS4	BAIT	H. sapiens	Affinity Capture-MS	Liu X (2021)	High	0.99	BioGRID
CSNK1G1	BAIT	H. sapiens	Affinity Capture-MS	Huttlin EL (2021/pre-pub)	High	1	BioGRID
PCDHB5	BAIT	H. sapiens	Affinity Capture-MS	Huttlin EL (2021/pre-pub)	High	0.8683	BioGRID
TMEM174	BAIT	H. sapiens	Affinity Capture-MS	Huttlin EL (2021/pre-pub)	High	0.8238	BioGRID
TTYH1	BAIT	H. sapiens	Affinity Capture-MS	Huttlin EL (2021/pre-pub)	High	0.9997	BioGRID
MARCH2	BAIT	H. sapiens	Affinity Capture-MS	Huttlin EL (2021/pre-pub)	High	0.9994	BioGRID
HLA-A	BAIT	H. sapiens	Affinity Capture-MS	Huttlin EL (2021/pre-pub)	High	0.974	BioGRID

Table S7

KEGG pathway enrichment analysis for RNF149-interacting proteins

#	Pathway	P-value	FDR
1	Cytokine-cytokine receptor interaction	2.11E-08	3.77E-06
2	Cell adhesion molecules	1.62E-05	0.00110144
3	Th1 and Th2 cell differentiation	1.85E-05	0.00110144
4	Signaling pathways regulating pluripotency of stem cells	7.28E-05	0.003256938
5	Viral myocarditis	9.85E-05	0.003527346
6	Th17 cell differentiation	3.99E-04	0.011897338
7	Autoimmune thyroid disease	5.06E-04	0.012951688
8	Phagosome	6.26E-04	0.013998211
9	Calcium signaling pathway	8.34E-04	0.016585917
10	TGF-beta signaling pathway	0.001136199	0.020337965
11	Allograft rejection	0.001252528	0.020382042
12	Hematopoietic cell lineage	0.001486765	0.022177584

P-value is calculated using hypergeometric test and adjusted by false discovery rate (FDR) correction.
The cutoff of significance is adjusted P-value<0.05. The lower P-value indicates the more significant enrichment.

Table S8

Transcriptome analysis of mRNA expression alterations of RNF-149-binding protein candidates in RNF149KO infarcted hearts

Gene name	log2FoldChange vs WT-MI	P-value
Ifngr1	-0.031229568	0.68259359
Crlf2	0.003573492	0.964892309
Osmr	0.217630226	0.000924776
Il4ra	0.172124447	0.129510205
Il3ra	0.277104623	0.00248508

Table S9

Echocardiographic parameters of WT and RNF149KO mice administrated with AAV-F4/80-NC or AAV-F4/80-shIFNGR1 14 days post-MI

Group	WT+NC	WT+IFNGR1KD	RNF149KO+NC	RNF149KO+IFNGR1KD
n	8	9	8	8
LVID;s (mm)	3.938±0.0888	3.293±0.0521 p=2.478E-05 **	4.884±0.1171 p=4.094E-08 ##	3.576±0.0586 p=3.196E-11 ††
LVID;d (mm)	4.468±0.1047	3.924±0.0488 p=0.0014 **	5.285±0.1321 p=6.952E-06 ##	4.186±0.0740 p=2.728E-08 ††
FS (%)	11.84±0.7124	16.09±0.5930 p=0.0009 **	7.576±0.3850 p=0.0014 ##	14.53±0.9894 p=9.145E-07 ††
EDV (μl)	91.42±5.091	66.99±1.923 p=0.0066 **	136.1±7.607 p=2.834E-06 ##	78.23±3.335 p=2.010E-08 ††
ESV (μl)	67.80±3.696	44.05±1.639 p=0.0005 **	113.4±6.124 p=1.332E-08 ##	53.72±2.170 p=3.205E-11 ††
EF (%)	25.71±1.393	34.33±1.147 p=0.0005 **	16.70±0.7934 p=0.0005 ##	31.10±1.889 p=2.810E-07 ††
HR (bpm)	563±13	564±14	577±9	569±10

Results are presented as mean ± SEM. Data were analyzed using two-way ANOVA with Bonferroni's multiple comparisons test.
** p versus WT+NC, ## p versus WT+NC, †† p versus RNF149KO+NC.
LVID;s = left ventricular internal diameter at end-systole; LVID;d = left ventricular internal diameter at end-diastole;
FS = fractional shortening; EF = ejection fraction; EDV = end-diastolic volume; ESV = end-systolic volume; HR = heart rate.

Table S10

Clinical characteristics of control subjects and patients with acute MI

Type	Etiology	Sex	Age	Diabetes	Hypertension	Smoking history	Drinking history
Control 1	Car accident	M	48	No	No	Never	Never
Control 2	Car accident	M	37	No	No	Never	Never
Control 3	Trauma	M	50	No	No	Former	Never
Control 4	Trauma	M	54	No	No	Former	Former
Control 5	Car accident	F	51	Yes	Yes	Never	Never
Hu-MI1	AMI	M	57	No	No	Former	Never
Hu-MI2	AMI	M	59	No	No	Former	Former
Hu-MI3	AMI	M	79	No	Yes	Never	Never
Hu-MI4	AMI	M	66	Yes	Yes	Never	Never
Hu-MI5	AMI	M	32	No	No	Former	Former

Hu-MI = human myocadial infarction; AMI = Acute Myocardial Infarction; M = male; F = female.

Table S11

Primers for real-time quantitative PCR

Gene	Species	Sense primer (5'-3')	Anti-sense primer (5'-3')	Amplicon sizes (bp)
Rnf149	Mus musculus	CACGCGGGAACAGGAAACATA	CGAGTACCAATCTCTATCCGCAT	116
Acta2	Mus musculus	CCCAGACATCAGGGAGTAATGG	TCTATCGGATACTTCAGCGTCA	104
Pecam1	Mus musculus	ACGCTGGTGCTCTATGCAAG	TCAGTTGCTGCCCATTCATCA	109
Col1a1	Mus musculus	GCTCCTCTTAGGGGCCACT	CCACGTCTCACCATTGGGG	103
TNFα	Mus musculus	CGTCGTAGCAAACCACCAA	GGGCAGCCTTGTCCCTTGA	165
Cxcl1	Mus musculus	ACTGCACCCAAACCGAAGTC	TGGGGACACCTTTTAGCATCTT	114
MMP3	Mus musculus	TCTGGGCTATACGAGGGCAC	ACCCTTGAGTCAACACCTGGA	232
TLR9	Mus musculus	ACGGGAACTGCTACTACAAGA	CCCAGCTTGACAATGAGGTTAT	184
TLR2	Mus musculus	CACCACTGCCCGTAGATGAAG	AGGGTACAGTCGTCGAACTCT	148
TLR4	Mus musculus	TTTGACACCCTCCATAGACTTCA	GAAACTGCAATCAAGAGTGCTG	114
Nlrp3	Mus musculus	ATCAACAGGCGAGACCTCTG	GTCCTCCTGGCATACCATAGA	96
IL-1β	Mus musculus	GCTGCTTCCAAACCTTTGACC	GAGTGATACTGCCTGCCTGAA	101
IL-12a	Mus musculus	TGCCTTGGTAGCATCTATGAGG	CGCAGAGTCTCGCCATTATGAT	167
IL-12b	Mus musculus	GTCCTCAGAAGCTAACCATCTCC	CCAGAGCCTATGACTCCATGTC	211
IL-6	Mus musculus	TCTATACCACTTCACAAGTCGGA	GAATTGCCATTGCACAACTCTTT	88
NOS2	Mus musculus	ACATCGACCCGTCCACAGTAT	CAGAGGGGTAGGCTTGTCTC	177
S100a8	Mus musculus	AAATCACCATGCCCTCTACAAG	CCCACTTTTATCACCATCGCAA	165
S100a9	Mus musculus	GCACAGTTGGCAACCTTTATG	TGATTGTCCTGGTTTGTGTCC	92
MMP9	Mus musculus	GCAGAGGCATACTTGTACCG	TGATGTTATGATGGTCCCACTTG	229
IL-23a	Mus musculus	AATAATGTGCCCCGTATCCAGT	GCTCCCCTTTGAAGATGTCAG	142
CCL2	Mus musculus	TTAAAAACCTGGATCGGAACCAA	GCATTAGCTTCAGATTTACGGGT	121
Csf3	Mus musculus	ATCCCGAAGGCTTCCCTGAGTG	AGGAGACCTTGGTAGAGGCAGA	101
Fas	Mus musculus	CTGCGATTCTCCTGGCTGTGAA	CAACAACCATAGGCGATTTCTGG	130
Arg1	Mus musculus	CTCCAAGCCAAAGTCCTTAGAG	AGGAGCTGTCATTAGGGACATC	185
Mgl2	Mus musculus	TTAGCCAATGTGCTTAGCTGG	GGCCTCCAATTCTTGAAACCT	101
YM1	Mus musculus	CAGGTCTGGCAATTCTTCTGAA	GTCTTGCTCATGTGTGTAAGTGA	197
MSR1	Mus musculus	TTCACTGGATGCAATCTCCAAG	CTGGACTTCTGCTGATACTTTGT	169
Tgfb1	Mus musculus	CTTCAATACGTCAGACATTCGGG	GTAACGCCAGGAATTGTTGCTA	142
MRC1	Mus musculus	CTCTGTTCAGCTATTGGACGC	CGGAATTTCTGGGATTCAGCTTC	132
CD36	Mus musculus	AGATGACGTGGCAAAGAACAG	CCTTGGCTAGATAACGAACTCTG	83
Fizz1	Mus musculus	CCAATCCAGCTAACTATCCCTCC	CCAGTCAACGAGTAAGCACAG	188
IL-10	Mus musculus	AGCCTTATCGGAAATGATCCAGT	GGCCTTGTAGACACCTTGGT	229
Ifngr1	Mus musculus	TGACTATGCACGGTCAAAAGAG	ATTCACAACGACTTCAGGGTG	130
Ifng	Mus musculus	ATGAACGCTACACACTGCATC	CCATCCTTTTGCCAGTTCCTC	182
Trim13	Mus musculus	CTACCTGCCGTAAGGAAACCT	CCACGATACCCTTTAGGGAGTA	75
VEGFα	Mus musculus	CTGCTGTAACGATGAAGCCCTG	GCTGTAGGAAGCTCATCTCTCC	119
GAPDH	Mus musculus	AGGTCGGTGTGAACGGATTTG	TGTAGACCATGTAGTTGAGGTCA	123